6-21-2016 12:00 AM

Structure and Function Relationships between ATPase Family, AAA Domain Containing Protein 5, Proliferating Cell Nuclear Antigen, and USP1-Associated Factor 1

Tam T. Bui
The University of Western Ontario

Supervisor
Dr. Hong Ling
The University of Western Ontario

Graduate Program in Biochemistry
A thesis submitted in partial fulfillment of the requirements for the degree in Master of Science

ABSTRACT

The genome is constantly damaged by intracellular and extracellular factors. At sites of DNA damage, replication forks are stalled, leading to monoubiquitination of proliferating cell nuclear antigen (PCNA). Monoubiquitination of PCNA promotes the switch from regular high-fidelity polymerases to Y-family polymerases for bypassing damaged DNA. Prolonged replication by these polymerases may lead to increased mutagenesis, so tight regulation of this process is required. ATAD5 recruits a deubiquitinase complex consisting of ubiquitin-specific protease 1 (USP1) and USP1-associated factor 1 (UAF1) to control PCNA monoubiquitination. The mechanism by which ATAD5 and PCNA interact has been previously unexplored. We show through biochemical and structural studies that ATAD5 contains a non-canonical PCNA-interacting protein motif that interacts with PCNA in the low μM range. Our structural studies indicate that the binding of ATAD5's PIP Box to PCNA is topologically conserved with respect to canonical PIP Boxes from other proteins. Furthermore, we detected we interactions between ATAD5's and UAF1's protein interacting motifs. This suggests that ATAD5 acts as an adapter between PCNA and the UAF1-USP1 deubiquitinase complex. Characterization of these interactions will increase our understanding of DNA damage tolerance and may lead to the design of better cancer therapeutics.

Keywords: PCNA, UAF1, ATAD5, PIP Box, DNA repair, DNA lesions, SUMO-like

ACKNOWLEDGEMENTS

I would like to thank my supervisor, Dr. Hong Ling for providing me with the opportunity to be a part of this project, as well as for her guidance and support throughout my time as her student. I have gained invaluable experience within and out of the lab that will surely be useful in my future endeavours. I would also like to thank my advisory committee members, Dr. Brian Shilton and Dr. Chris Brandl for their continued support, feedback, and advice during meetings. I would also like to thank Dr. Chris Brandl for the yeast strain and plasmids used in the two-hybrid experiments, sharing his expertise in yeast, and space in his lab for me to work.

To Dr. Guangxing Xing, for offering his aid and advice in troubleshooting experiments and maintaining the lab. A special thanks to Dr. Vikash Jha for all of his help throughout the crystallization process and structure building and refinement.

To the past and current members of the lab, Dr. Chuanbing Bian, Lizhen Guo, Andy Liu, Ryan Martin, Rebecca Earnshaw, Josh Brar, Sam Chu, Ian Wei, and all of the other undergraduate students, you have made my graduate experience a special one. I would also like to thank Lee-Ann Briere for your training and advice, I always look forward to your stories.

To my friends from graduate school and the University of Guelph, especially Michelle Dubinsky, Dee Laxton and Erin Garbett, for always lending me an ear to talk to and a shoulder to lean on. Finally, I would like to thank my parents for their support and encouragement, I would not be who I am without them.

TABLE OF CONTENTS

LIST OF TABLES

LIST OF FIGURES

LIST OF ABBREVIATIONS AND ACRONYMS

Amino Acids

Ala (A)	Alanine
Arg (R)	Arginine
Asn (N)	Asparagine
Asp (D)	Aspartic acid
Cys (C)	Cysteine
Gln (Q)	Glutamine
Glu (E)	Glutamate
Gly (G)	Glycine
His (H)	Histidine
Ile (I)	Isoleucine
Leu (L)	Leucine
Lys (K)	Lysine
Met (M)	Methionine
Phe (F)	Phenylalanine
Pro (P)	Proline
Ser (S)	Serine
Thr (T)	Threonine
Trp (W)	Tryptophan
Tyr (Y)	Tyrosine
Val (V)	Valine

AD	Activating domain
ATAD5	ATPase family, AAA domain-containing protein 5
BD	Binding domain
DDT	DNA damage tolerance
DNA	Deoxyribonucleic acids
dNTP	Nucleoside triphosphate
DTT	Dithiothreitol
DUB	Deubiquitinase

E. coli	*Escherichia coli*
EDTA	Ethylenediaminetetraacetic
g	Times gravity
GST	Glutathione S-transferase
IDCL	Interdomain connecting loop
IMAC	Immobilized metal affinity chromatography
IPTG	Isopropyl β-D-1-thiogalactopyranoside
ITC	Isothermal titration calorimetry
K_d	Dissociation constant
kDa	KiloDalton
M-PIPE	Mutagenic primer incomplete polymerase extension
MBP	Maltose binding protein
$MgCl_2$	Magnesium chloride
MW	Molecular Weight
NaCl	Sodium chloride
PCNA	Proliferating cell nuclear antigen
PCR	Polymerase chain reaction
PEG	Polyethylene Glycol
PIP Box	PCNA-interacting protein motif
PIPE	Primer incomplete polymerase extension
PMSF	Phenylmethylsulfonyl fluoride
Pol	Polymerase
RFC	Replication factor C
rpm	Rotations per minute
SDS-PAGE	Sodium dodecyl sulfate poly acrylamide gel electrophoresis
SIM	SUMO-interacting motif
SLD	SUMO-like domain
SUMO	Small ubiquitin-like modifier
TLS	Translesion synthesis
UAF1	USP1-associated factor 1
ub	Ubiquitin

UBM	Ubiquitin binding motif
ubPCNA	Monoubiquitinated PCNA
UBZ	Ubiquitin binding zinc finger motif
USP1	Ubiquiti specific protease 1
β-me	β-mercaptoethanol
USP1	Ubiquitin-specific protease 1

CHAPTER 1: INTRODUCTION

1.1 Translesion DNA Synthesis

Faithful replication of a cell's genetic material during replication is essential in order to pass genetic material from one generation to the next; however, DNA-damaging agents constantly injure the genome. High fidelity replication of the cell's genetic material is normally carried out through the combination of accurate DNA polymerases and DNA mismatch repair (1). These high-fidelity DNA polymerases have evolved mechanisms to strongly favor correct dNTP incorporation opposite to the template strand during replication (1). However, these polymerases are unable to replicate past damaged DNA, and are stalled at these sites (2). Stalled replication forks are dangerous as they can collapse, causing chromosomal breaks and genomic instability (3).

Cells belonging to all branches of life possess DNA damage tolerance (DDT) pathways in order to survive in the presence of DNA-polymerase blocking lesions and to restart stalled replication forks (4). One of the DDT pathways is the translesion synthesis (TLS) pathway, which involves the use of specialized DNA polymerases, most of which belong to the Y-family (5). Y-family polymerases differ from other polymerases in that they are able to replicate past DNA lesions and have reduced fidelity on undamaged templates (6). Prolonged replication by these low-fidelity polymerases could have deleterious consequences arising from mutations, so it is crucial that their activity is strictly regulated (6). The specific mechanism in which different polymerases are loaded on and off of the replication fork involves post-translational modification of proliferating cell nuclear antigen (PCNA) (7).

1.2 Proliferating Cell Nuclear Antigen

PCNA is a DNA sliding clamp with multiple functions in DNA replication and repair. Two separate groups first identified PCNA independently from each other. The first group, Miyachi et al. (1978), observed an auto-antigen in the nucleus of dividing cells from patients with systemic lupus erythematosus and named it PCNA (8). The second group, Bravo and Celis (1980), identified a protein that was synthesized during the S-phase of the cell cycle using two-dimensional gel electrophoresis and named it cyclin (9). Work by Mathews et al. (1984) later demonstrated that the two proteins discovered by these groups were the same (10). Today the protein is called PCNA, as the term cyclin is now reserved for a family of proteins involved in cell cycle regulation (11).

PCNA has functions at various levels of DNA metabolic pathways while unbound or bound to DNA. When unbound to DNA, PCNA promotes the localization of replication factors with PCNA-binding domains to replication factories (12). When bound to DNA, PCNA directs proteins involved in DNA replication, repair, modification, and chromatin modeling (12). PCNA is the processivity factor of Polδ and is therefore the functional homologue of other processivity factors such as the β subunit of *E. coli* DNA polymerase III holoenzyme (Pol III) and the gene-45 product of bacteriophage-T4 (11). Stukenberg et al. (1991) first established the concept that a processivity factor functions by encirculating DNA through experiments on the β subunit of *E. coli* Pol III (13). They demonstrated that the β subunit bound tightly to nicked circular plasmid, however, the clamp dissociates off of DNA by sliding over the ends upon linearization of the plasmid (13). The determination of the crystal structure of the β subunit confirmed these studies and revealed that it is a homodimeric ring (14).

1.2.1 Human PCNA Structure

The ortholog of the β subunit of Pol III in eukaryotes is PCNA. Although the sequence similarity between these two proteins is limited, they are structurally similar. Human PCNA consists of three identical monomers instead of two (Figure 1A) (15). Each monomer of human PCNA contains two similar domains, giving the complete protein a six-fold pseudo symmetry (Figure 1C) (12). Each of the domains is composed of a series of antiparallel β strands forming curved β sheets. Six curved β sheets make up a donut-like scaffold. Two alpha helices from each domain face inward approximately perpendicular to the face of the ring to form a cylindrical inner cavity with a diameter of about 34 Å. This is much larger than the diameter of double stranded B DNA (20 Å). Although PCNA has a net negative charge, the inner cavity is electrostatically positive. Up to 10 positively charged amino acid side chains face toward the center from the alpha helices, however, there are only three negatively charged amino acids to counteract the charge. The positively charged ring forms favourable interactions through the solvent to the negatively charged phosphodiester backbone of DNA (12).

PCNA has a distinct back and front face (Figure 1B). The front face of PCNA is oriented in the direction of DNA synthesis and contains structural elements that are involved in many protein interactions (16). The C-terminal tails of the monomers face frontward along with an interdomain connecting loop (IDCL) which links the N- and C-terminals of each monomer (12). The IDCL covers a hydrophobic pocket, which can be "plugged" by proteins containing a PCNA-interaction protein motif (PIP box) (15).

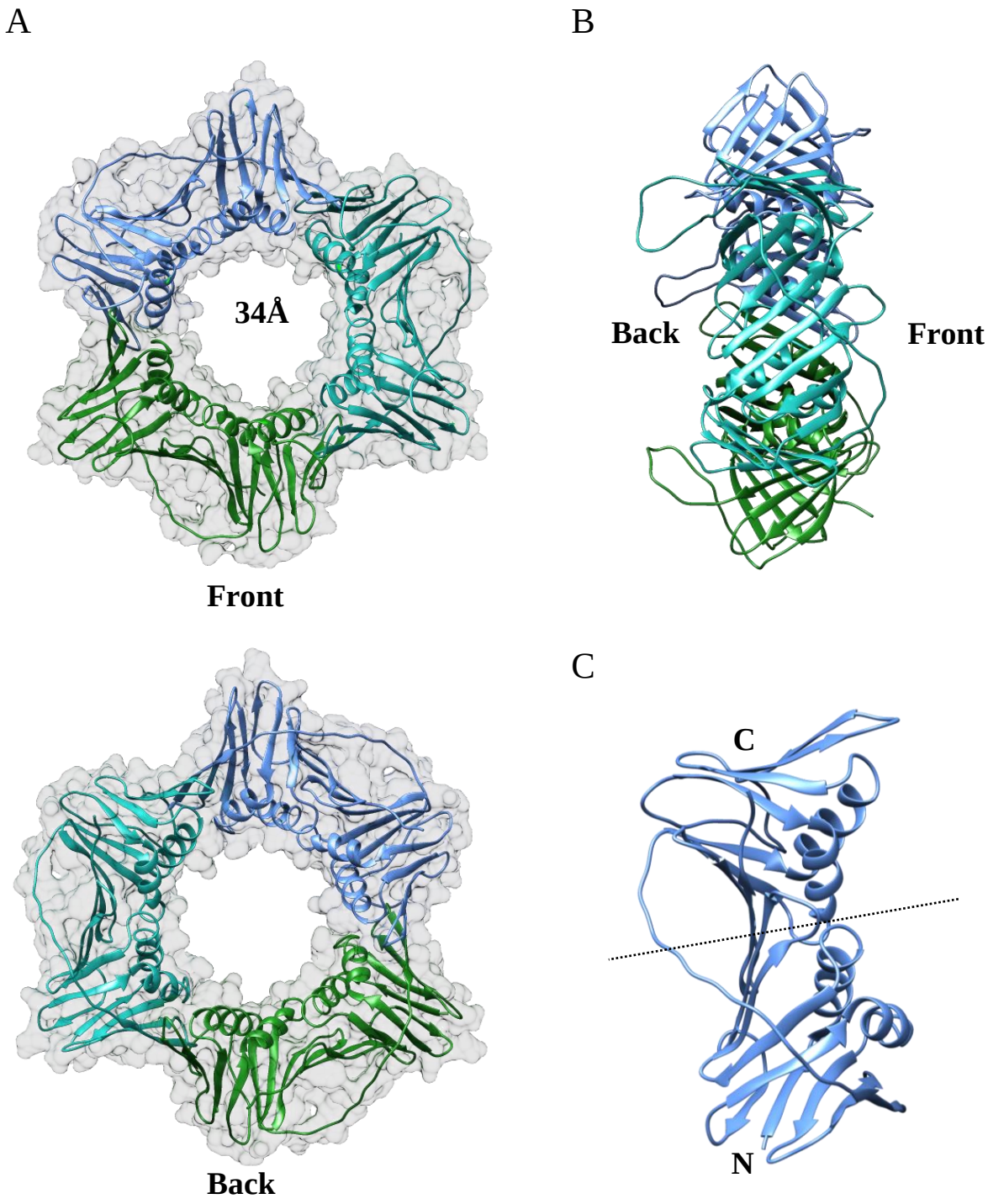

Figure 1. Structure of native human PCNA (PDB ID: 1W60). Each monomer is coloured differently. A) Cartoon representation with transparent surface of the front (top) and back (bottom) view of PCNA showing the diameter of the inner ring. B) Side view of PCNA with the front and back labelled. C) Front view of PCNA monomer. The two similar globular domains have been divided by a dotted line. N- and C- terminals are indicated in bold.

1.2.2 PCNA-interacting protein motif (PIP box)

Virtually all proteins that interact with PCNA contain a PCNA-interacting protein motif termed the "PIP box". The consensus binding motif of the PIP box is: Qxx[Ψ]xx[ϑ][ϑ] (x being any amino acid, ψ being the hydrophobic residues L, M, or I and ϑ being the aromatic residues F or Y (17). In some cases, instead of being C-terminally flanked by xx[ϑ][ϑ], the Qxx[Ψ] motif can be flanked by KAx instead (18). A sequence alignment of human proteins that interact with PCNA is shown in Figure 2. Gulbis *et al.* (1996) first published a crystal structure that revealed how the PIP box interacts with PCNA using a peptide derived from $p21^{WAF1/CIP1}$ (p21), an inhibitor of the cyclin-dependent kinases that control the initiation of S phase and DNA replication (19). This peptide binds PCNA with high affinity, the interaction has a K_d in the low nanomolar range (15, 20). The PIP box of this peptide was shown to form an alpha helix that acts as a hydrophobic plug, docking into the hydrophobic pocket on PCNA. Furthermore, the C-terminal of this peptide forms a β sheet structure that makes extensive contacts with the IDCL (15). Proteins that interact with PCNA through a PIP box may also use additional regions for interaction (21). Because many proteins that contain PIP boxes bind to PCNA in the same region, the binding is often mutually exclusive and competitive (21).

Many of the pathways which PCNA is part of involves the transfer of DNA from one enzyme to another. For example, during Okazaki fragment processing, FEN1 must cleave the 5' flap on DNA before DNA ligase can patch the nick (22). One possibility of how this occurs is that PCNA acts as a "toolbelt", binding all the necessary enzymes required to facilitate the transfer of the substrate (22). This has been observed in

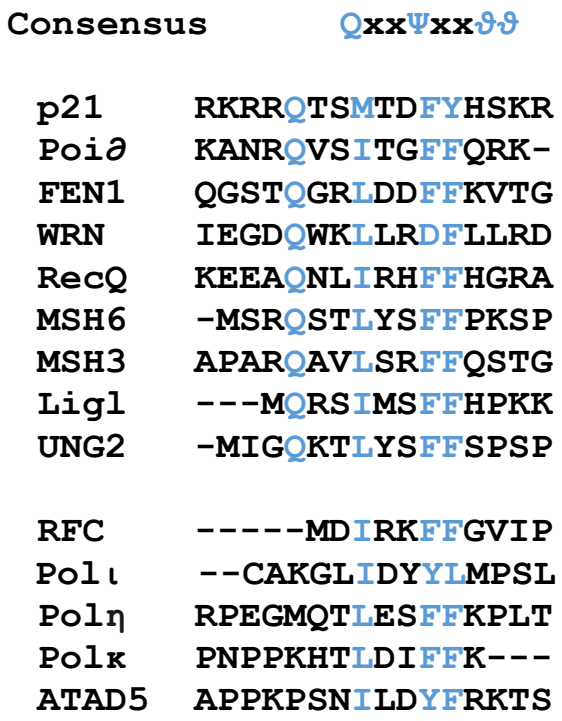

Figure 2. Sequence alignment of human proteins containing PIP boxes. The consensus sequence is shown with the alignment, where x being any amino acid, ψ being the hydrophobic residues L, M, or I and ϑ being the aromatic residues F or Y. Canonical PIP box residues are coloured blue at positions 1, 4, 7 and 8. Canonical and non-canonical PIP boxes are separated.

S. solfataricus where a PCNA heterotrimer simultaneously binds to DNA polymerase, FEN1, and DNA ligase (23). However, There is currently no clear evidence that suggests eukaryotic PCNA functions as a toolbelt, however, it is likely (22).

1.2.3 Post-translational modification of PCNA

PCNA is post-translationally modified in response to stalling of the replication fork via sumoylation or monoubiquitination (24). As previously mentioned, prolonged stalling of the replication fork during DNA replication is dangerous as it can collapse. This causes double-stranded breaks and gross chromosomal rearrangements which may lead to cell death (3). Restart of the replication fork is possible through post-translational modification of PCNA and subsequent activation of one of two DDT pathways. These pathways include the homologous recombination repair pathway through sumoylation of K164 or the post-replication repair pathway via monoubiquitination of the same lysine residue (25, 26). As seen in Figure 3A, monoubiquitination of K164 is carried out by E2 ubiquitin conjugating enzyme Rad6 and E3 ubiquitin ligase Rad18 (Rad6/Rad18 complex) in the RAD6 pathway (25). Rad18 recruits the ubiquitination machinery to DNA-bound PCNA through interactions with Rad6, PCNA, and DNA (27). The structure of mono-ubiquitinated PCNA is shown in Figure 3B.

Monoubiquitinated PCNA (ubPCNA) has been proven to promote TLS carried out by Y-family polymerases. In addition to the PIP box motif, these polymerases also contain ubiquitin-binding motifs (UBMs) or ubiquitin-binding zinc fingers (UBZ) which are able to interact with the ubiquitin moiety and increase its affinity to ubPCNA (24). Tight regulation of TLS polymerases is required, as prolonged replication by these error-prone

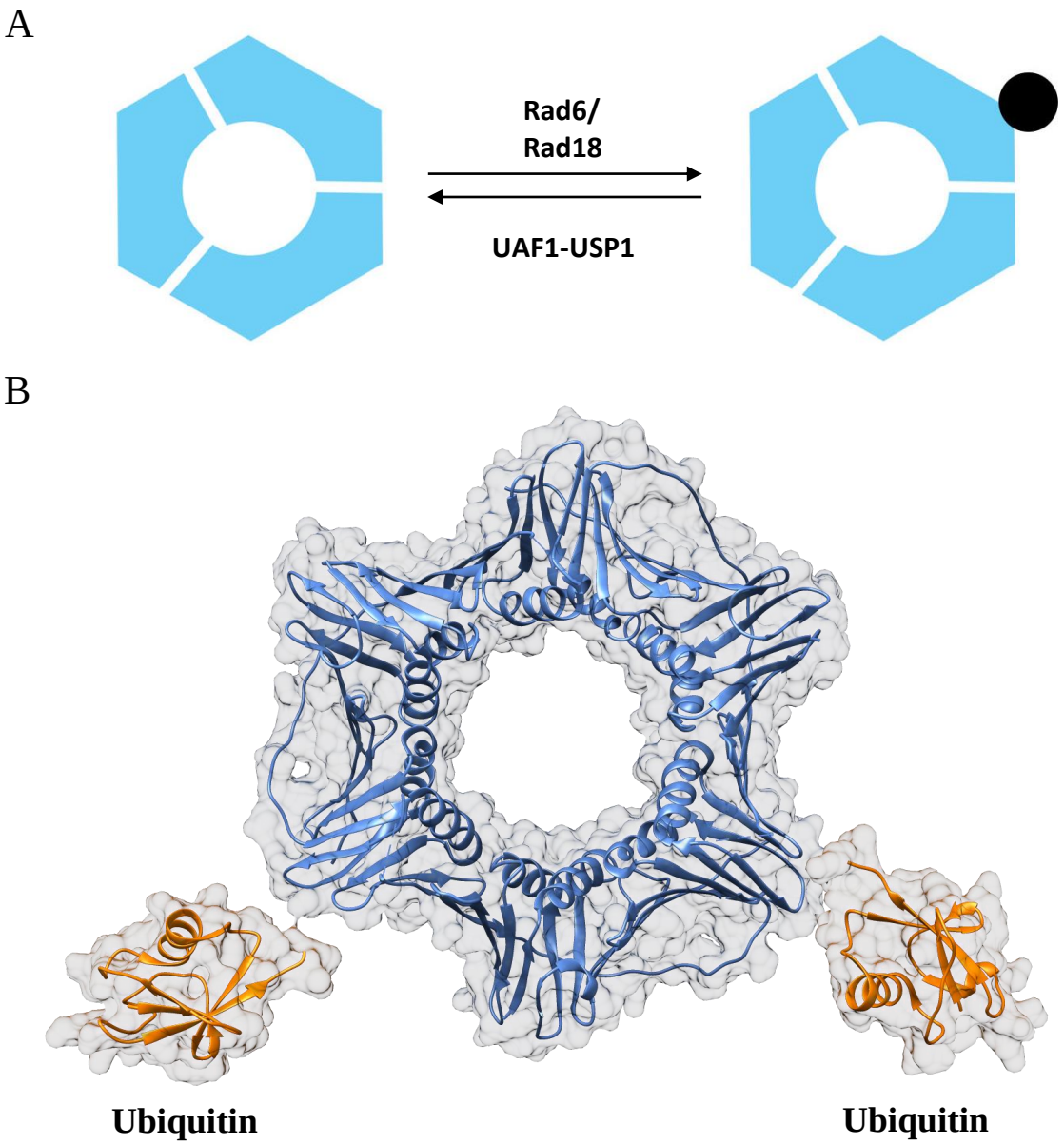

Figure 3. PCNA ubiquitination is regulated by the RAD6 pathway and the UAF1-USP1. A) PCNA is monoubiquitinated through the Rad6 pathway and deubiquitinated through the recruitment of the UAF1-USP1 deubiquitinase (DUB) complex. B) Structure of monoubiquitinated PCNA (PDB ID: 3TBL). Ubiquitin molecules (orange) are covalently linked to K164 of PCNA (blue) on two of three monomers.

polymerases may lead to increased mutagenesis. Zhuang et al. (2008) demonstrated that the switching from the TLS polymerase η (Polη) to the normal high-fidelity Polδ is inhibited by the ubiquitin moiety on PCNA (28). This suggests that deubiquitination is required for the normal high-fidelity polymerase to switch back to DNA synthesis after lesion bypass. Ubiquitin specific protease 1 (USP1) was identified in a siRNA screen as a putative deubiquitinase (DUB) for PCNA (29).

1.3 Ubiquitin-Specific Protease 1 (USP1) and USP1 Associated Factor (UAF1) Complex

DUB enzymes control deubiquitination of human proteins. Although 95 distinct proteins belong to this family of proteins, many of their functions are unknown (30). DUBs are cysteine proteases that remove ubiquitin from their substrate, either from mono- or poly- ubiquitinated proteins or from linear ubiquitin polypeptides (29).

USP1 is a DUB that negatively regulates PCNA monoubiquitination *in vivo* and *in vitro* (29). Upon DNA damage, transcription of USP1 is immediately turned off leading to a rapid decay of USP1. This allows for PCNA to become monoubiquitinated, which is essential for translesion synthesis (31). Knockdown of USP1 increases mutation frequency during DNA replication and causes increased levels of ubPCNA (29). USP1 is activated through interaction with USP1 associated factor 1 (UAF1). UAF1 stabilizes USP1 and is essential for its deubiquitinating activity. UAF1 is also part of the Fanconi Anemia pathway in charge of FANCD2 deubiquitination (30). USP1 alone has very low enzymatic activity, however when it is part of a complex with UAF1, its activity increases 35-fold. This increase is due to an 18-fold increase in catalytic turnover, and 2-fold increase in the

proteins affinity to its substrate (31). The UAF1-USP1 DUB complex is likely recruited to ubiquitinated PCNA through its interaction with ATAD5 (32).

UAF1 has an N-terminal WD40 domain containing eight WD40 propeller sequences and two consecutive SUMO-like domains (SLD1 and SLD2) in its C-terminal (Figure 4). The N-terminal binds and stimulates USP1's ubiquitin protease activity (33). Of the two SLDs in the C-terminal of UAF1, only the second SLD interacts with a SUMO-interacting motif (SIM) on ATAD5.

1.4 ATPase family, AAA domain-containing protein 5 (ATAD5)

ATPase family, AAA domain-containing protein 5 (ATAD5) is the human homolog of the yeast protein enhanced levels of genomic stability 1 (Elg1). Elg1 is divided into three main domains: an extended N-terminal domain, a central AAA+ ATPase domain, and a C-terminal domain (Figure 4) (34). Elg1 was originally identified in a screen for suppressors of chromosomal instability and is a protein which participates in telomere maintenance in yeast (35, 36). Elg1 has also been suggested to form an RFC-like complex, which functions in stabilization of the DNA replication fork. This RFC-like complex unloads PCNA from DNA following Okazaki fragment ligation in DNA lagging strand synthesis (37, 38). Knockdown of ATAD5 in mammalian cells leads to spontaneous chromosomal breaks, increased levels of recombination and aberrations in the chromosome such chromosomal fusions and inversions (39, 40).

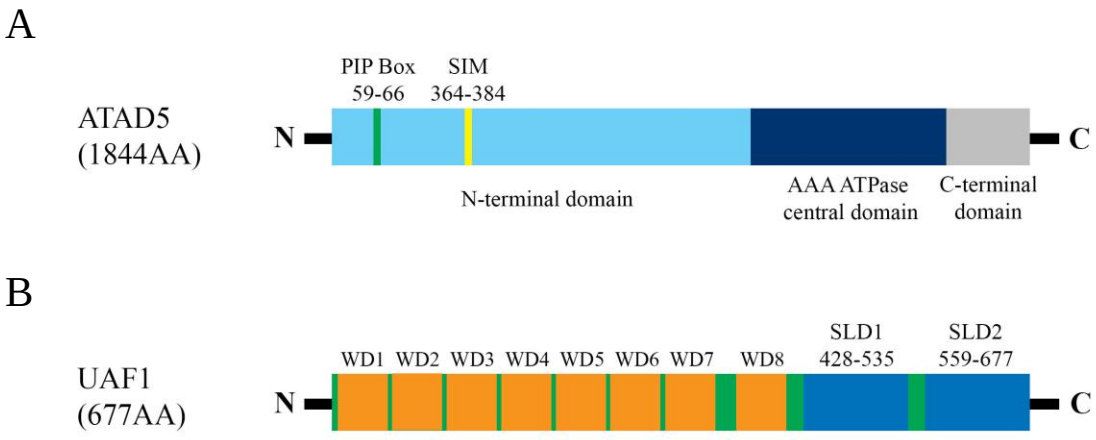

Figure 4. Schematic of ATAD5 and UAF1. A) Schematic diagram of ATAD5 with PCNA-interacting Protein (PIP) Box and sumo-interacting protein motif (SIM) coloured green and yellow respectively. B) Schematic diagram of UAF1 with WD domains coloured orange and sumo-like domains coloured blue.

Knockdown of ATAD5 also causes PCNA and ubPCNA accumulate on DNA (41). Consequently, the lifespan of replication factories (that use PCNA as a scaffold) is extended, and remains well into G2 phase of cell division (41). The increase in PCNA suggests that ATAD5 may interact with the core subunits of the RFC (rfc2-5) to form an RFC-like complex, which is responsible for unloading PCNA similar to its yeast homologue (41). Any binding of ATAD5 to PCNA has yet to be investigated, however, a non-canonical PIP box motif has been shown to interact with PCNA in yeast (26, 34). The accumulation of ubPCNA on DNA is due to ATAD5's role in recruiting the UAF1-USP1 DUB complex.

ATAD5 interacts with UAF1 through a interaction similar to how the small ubiquitin-like molecule (SUMO) interacts with a SIM: a SIM located in the N-terminal of ATAD5 interacts with a SUMO-like domain (SLD) of UAF1 (32). The SIM consists of a hydrophobic core, consisting of 3-4 aliphatic residues, juxtaposed to a negatively charged cluster of acidic residues (42). The binding site of ATAD5 (KSNVVIQEEELELAVLE) conforms to the consensus sequence of a SIM, and it is highly conserved among species (43).

We have previously identified a putative PIP box motif in our lab in the N-terminal of ATAD5 (Figure 2). Work done by Haley McConkey showed that a short peptide containing this putative motif fused to GST was able to interact with PCNA in an affinity pull-down assay. Furthermore, she showed that mutations to the two hydrophobic residues at position 7 and 8 of this motif abolished the binding.

1.5 Scope of thesis

Although it is proposed that ATAD5 functions to unload PCNA and recruit the UAF1-USP1 DUB complex to ubPCNA, little is known about the interaction between ATAD5 and PCNA. In yeast, Elg1 binds to PCNA through a non-canonical PIP box similar to that of rfc1, a subunit of the RFC complex. PCNA has many binding partners, and regulation of which protein binds at a given time is essential for certain cellular processes such as the post replication repair or DDT pathways and DNA replication to occur. Elucidation of the structural basis in which ATAD5 binds to PCNA and UAF1 can then be applied to other proteins that bind to it.

The goal of this study is to elucidate the physical and functional relationships between the binding of the human proteins: ATAD5, PCNA and UAF1, through structural and biochemical methods. The ultimate objective of this study is to contribute to our understanding of how the cell is able to recruit Y-family polymerases to stalled replication forks arising from DNA lesions and facilitate switching from high- to low- and back to high-fidelity polymerases.

1.6 Hypothesis

As seen in the sequence alignment of ATAD5's PIP box with other human PCNA-binding proteins, ATAD5 contains a putative PIP box motif close to its N-terminal that resembles those of the Y-family polymerases and rfc1 (Figure 2). Furthermore, ATAD5 contains a SIM-like motif that interacts with a SLD on UAF1. Therefore, we propose that ATAD5 serves as an adaptor protein (Figure 5) that is able to bind both PCNA and UAF1. We aim to characterize the physical interaction between the PIP box and SIM motif on the

N-terminal of ATAD5 with PCNA and UAF1 through various biochemical methods. Finally, we aim to elucidate the structural features of the binding between these proteins through macromolecular crystallographic techniques.

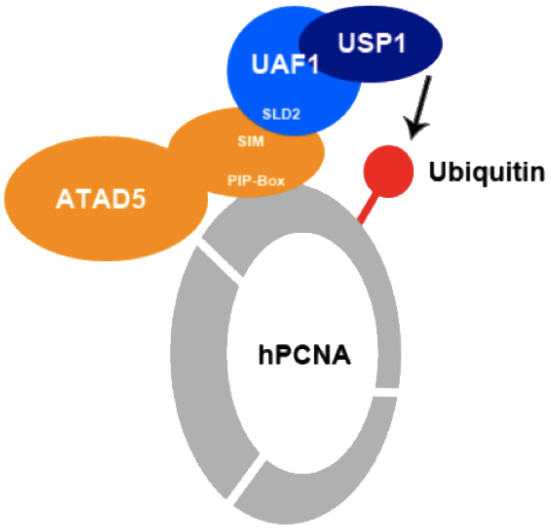

Figure 5. Schematic diagram of ATAD5 acting as an adaptor protein between monoubiquitinated human PCNA and the UAF1-USP1 DUB complex. ATAD5 contains a sumo-interacting motif (SIM) that interacts with the second sumo-like domain (SLD2) on UAF1 as well as a PCNA-interacting protein motif (PIP box) that interacts with PCNA.

CHAPTER 2: MATERIALS AND METHODS

2.1.1 Bacterial strains and plasmids

The plasmid expressing full-length wild-type PCNA was previously subcloned from pAVR38, a generous gift from Dr. Roger Woodgate of the National Institutes of Health (Maryland, USA), into pET22b. The pMCSG9, pMCSG10, pBluescriptR_UAF1 and pANT7-cGST-ATAD5 plasmids were purchased from the PlasmID Repository (Harvard Medical School, Massachusetts, USA). Bacterial strain BL21(DE3) was commercially purchased from Novagen. The maps of the vectors used are available in the appendix (Figure I-II). A schematic diagram of the various domains from ATAD5 and UAF1 used in this study are depicted in Figure 4.

2.1.2 Yeast strains and plasmids

The PJ694A yeast strain, and pASI and pACT2 vectors were generously provided by Dr. Chris Brandl of the Schulich School of Medicine and Dentistry (Western University, Ontario, Canada).

2.1.3 List of buffers

Buffers used in the purification of proteins and experiments have been compiled in Table 1.

Table 1. Summary of buffers used in this study.*

Buffer	Used In	Components
Buffer A	PCNA purification	25 mM Tris pH 7.5, 1 mM EDTA, 7 mM β-Me, 0.01 % NP-40
Buffer B	PCNA purification	25 mM Tris pH 7.5, 1 mM EDTA, 7 mM β-Me, 0.01 % NP-40, 1 M NaCl
Buffer C	PCNA purification	50 mM NaAc pH 5.5, 10 % glycerol, 7 mM β-Me, 0.01 % NP-40
Buffer D	PCNA purification	50 mM NaAc pH 5.5, 10 % glycerol, 7 mM β-Me, 0.01 % NP-40, 1 M NaCl
Buffer E	PCNA purification	25 mM KH_2PO_4/K_2HPO_4 pH 7.0, 10 % glycerol, 1 mM DTT
Buffer F	PCNA purification	300 mM KH_2PO_4/K_2HPO_4 pH 7.0, 10 % glycerol, 1 mM DTT
Buffer G	PCNA purification	25 mM Tris pH 7.5, 150 mM NaCl, 10 % Glycerol, 1 mM EDTA, 1 mM DTT
ITC Buffer	ITC	25 mM HEPES pH 7.5, 150 mM NaCl, 5 mM β-Me
HIS Buffer A	MBP/GST-tagged Protein purification	25 mM Tris pH 7.5, 500 mM NaCl, 1 mM EDTA, 7 mM β-Me
HIS Buffer B	MBP/GST-tagged protein purification	25 mM Tris pH 7.5, 500 mM NaCl, 1 mM EDTA, 7 mM β-Me, 300 mM imidazole
Q Buffer A	MBP/GST-tagged Protein purification	25 mM Tris pH 7.5, 1 mM EDTA, 7 mM β-Me
Q Buffer B	MBP/GST-tagged Protein purification	25 mM Tris pH 7.5, 1 M NaCl, 1 mM EDTA, 7 mM β-Me
Pull-Down Buffer	Pull-down assays	25 mM HEPES pH 7.5, 150 mM NaCl, 1 mM EDTA, 5 mM β-Me
GST Elution Buffer	GST Purification	25 mM Tris pH 7.5, 200 mM NaCl, 1 mM EDTA, 7 mM β-Me, 10 mM reduced glutathione
MBP Elution Buffer	MBP Purification	25 mM Tris pH 7.5, 200 mM NaCl, 1 mM EDTA, 7 mM β-Me, 10 mM maltose

*The referred name is listed under the "Buffer" heading, with the corresponding experiment and components in the columns on the right.

2.1.4 Cloning of constructs used in yeast two-hybrid assay

Plasmids pASI-PCNA, pASI-UAF1_SLD2, pACT2-ATAD5_N250, pACT2-ATAD5_N498 were made through traditional "cut and paste" cloning. Appropriate gene segments were amplified with an addition of an appropriate restriction enzyme cut site by PCR using the appropriate forward and reverse primers summarized in Table 2. The cloning of these constructs followed a previously described protocol with minor modifications (44).

In brief, the amplification was carried out with 1 ng of DNA template, 500 pM of forward and reverse primer, 200 μM of dNTPs, and 1 U of *i*-MAX™ II DNA polymerase (iNtRON) in 20 μL reactions. An initial touchdown protocol was applied to avoid non-specific binding of the primer, followed by cycling conditions outlined by the manufacturer. The annealing temperature for the PCR products varied depending on the primers used (Table 2). The PCR products were then diluted and digested with BamHI and XhoI along with the vectors (pASI and pACT2) for 2 hours at 37 ^{o}C. The digested DNA was then purified from a 1.5 % agarose gel using the QIAquick® Gel Extraction Kit (Qiagen Inc.). The DNA was then ligated into the appropriate vectors with T4 DNA ligase (New England Biolabs Inc.) in a 3:1 molar ratio of insert to vector DNA. 5 μL of the ligation reaction was transformed into competent DH5α cells and grown overnight at 37 ^{o}C on LB agar plates supplemented with 100 μg/mL of ampicillin. The plasmids were then harvested from 3 mL cultures grown from single colonies and confirmed by DNA sequencing.

Table 2. Summary of constructs used for yeast two-hybrid experiments..*

Construct	Protein (Mutation)	Amino Acid Residues	$T_{Annealing}$ (°C)	Primers (Forward and Reverse)
pASI-PCNA	PCNA		64	5'- taatggatccatatgttcgaggcgcgcctg -3' 5'- gctagttattgctcagcgg -3'
pASI-UAF1_SLD2	UAF1	559-677	56	5'- ctgtacttccaatccatgcccaaattcaacaaaattcc -3' 5'- ttatccacttccaatttacgtggacttctgacggtaatg -3'
pASI-UAF1_SLD2M	UAF1 (K595E)	559-677	63	5'- ctccaagtccgagaagttatggaacatgtttatg -3' 5'- gttccataacttctcggacttggagcatgt -3'
pACT2-ATAD5_N250	ATAD5	2-250	55	5'- taatggatccatgtgggggtcctggccatg -3' 5'- ctgcatctcgagttaatctctagagtttgcatggc -3'
pACT2-ATAD5_N250M	ATAD5 (I62A, Y65A, and F66A)	2-250	67	5'- gcactggatgcagcaagaaagacttcacccacaaatgagaag -3' 5'- tgctgcatccagtgcattactaggttttggtggagcaaaaacc -3'
pACT2-ATAD5_N498	ATAD5 (2-498)	2-498	55	5'- taatggatccatgtgggggtcctggccatg -3' 5'- ctgcatctcgagttatcccctctctgtttttgcc -3'
pACT2-ATAD5_SIM	ATAD5	340-406	56	5'- taatggatcctaccccgaattttcttgaaacaaaagc -3' 5'- ctgcatctcgagttatgctttcataaattgctgtctttc -3'

*Original protein as well as length of expressed protein are described. Annealing temperatures and primers used are listed. Mutations are described in brackets and primers used for mutagenesis.

After confirming that the products are correct, mutations to pASI-UAF1_SLD2 and pACT2-ATAD5_N250 were introduced to make pASI-UAF1_SLD2M and pACT2-ATAD5_N250M. The mutagenesis of these two primers was completed using overlap extension PCR as previously described with minor modifications (45). The primers were designed according to the mutagenic primer-incomplete polymerase extension (M-PIPE) protocol (shown in Table 2 with the mutations underlined) (46).

Briefly, two reactions were set up for each mutation as previously described, however one reaction contained the forward primer for the insert and the reverse primer for mutagenesis, and the other reaction containing the opposite primer pairs. The two reactions were then digested with *DpnI* for 2 hours at 37 ^{o}C to break down the methylated template DNA. The two reactions were then purified from a 1.5 % agarose gel using the QIAquick® Gel Extraction Kit (Qiagen Inc.) and combined to be used as the template for the second PCR step. The same forward and reverse primers for insert amplification were used in the second PCR. The products were then digested with *BamHI* and *XhoI* and ligated into the appropriate vectors as previously described. Following transformation of the plasmids into competent DH5α cells, plasmids were extracted from 3 mL overnight cultures grown from single colonies. The plasmids were verified using DNA sequencing.

2.1.5 Cloning of constructs used for protein expression

The GST-fusion constructs pMCSG10-ATAD5_PIP, pMCSG10-ATAD5_PIPM and pMCSG10-p21 were previously prepared by Guangxing Xing. The GST-fusion construct pMCSG10-ATAD5_SIM and the MBP-fusion pMCSG9-UAF1_SLD2 were prepared using primer incomplete polymerase extension (PIPE) cloning as previously

described with modifications (46). All constructs used for protein expression are listed in Table 3 along with the appropriate primers used (where available).

In brief, the insert for each construct was amplified using PCR with primers adding sequences at the 5' and 3' ends complementary to the sequences added to the vectors. The vector was also amplified as well. The amplifications were carried out with 1ng of template DNA, 500 pM of forward and reverse primers, 200 μM of dNTPs, and 0.5 U of Q5 High-Fidelity DNA Polymerase (New England Biolabs Inc.). The Q5 High GC Enhancer (New England Biolabs Inc.) was added to the reactions to amplify the insert from pANT7-cGST-ATAD5. Touchdown PCR was used to amplify the products with an annealing temperature range from 65 ºC to 55 ºC. The products were then digested with *DpnI* for 2 hours at 37 ºC and only the vector was purified from a 0.7 % agarose gel using the QIAquick® Gel Extraction Kit (Qiagen Inc.). The inserts were then mixed with the vectors and incubated at room temperature for 5 minutes and on ice for 5 minutes. 5 uL of this mixture was then transformed into competent DH5α cells and grown overnight at 37 ºC. 3 mL cultures were grown from single colonies and the plasmids were harvested and verified by DNA sequencing.

The same mutation was made to UAF1's SLD2 domain in pMCSG9-UAF1_SLD2 as in pASI-UAF1_SLD2 using overlap extension PCR as previously described to create pMCSG9-UAF1_SLD2M.

Table 3. Summary of constructs used for protein expression and purification.

Construct	Protein (Mutation)	Amino Acid Residues	$T_{Annealing}$ (°C)	Primers (Forward and Reverse)
pMCSG10-p21	p21	-		
pMCSG10-ATAD5_PIP	ATAD5	51-75		
pMCSG10-ATAD5_PIPM	ATAD5 (Y65A and F66A)	51-75		
pMCSG10-ATAD5_SIM	ATAD5	340-406	55	5'- ctgtacttccaatcctctgatcctgagaatgaacag -3' 5'- ttatccacttccaatttaccaggtttcacagcttcag -3'
pMCSG9-UAF1_SLD2	UAF1	559-677	56	5'- ctgtacttccaatccatgcccaaattcaacaaaattcc -3' 5'- ttatccacttccaatttacgtggacttctgacggtaatg -3'
pMCSG9-UAF1_SLD2M	UAF1 (K595E)	559-677	63	5'- ctccaagtccgagaagttatggaacatgtttatg -3' 5'- gttccataacttctcggacttggagcatgt -3'

*Original protein as well as length of expressed protein are described. Annealing temperatures and primers used are listed where available. Mutations are described in brackets and primers used for mutagenesis.

2.2 Expression and purification

2.2.1 Expression and purification of PCNA

BL21(DE3) *E. coli* cells containing the pRARE plasmid were transformed with pET22b-hPCNA and incubated at 37 ^{o}C overnight. Colonies were picked and grown in a 50 mL starter culture of 2xYT media containing 100 μg/mL ampicillin and 25 μg/mL chloramphenicol. The starter culture was used to inoculate 1 L of 2xYT media with the same concentration of antibiotics, supplemented with 6 mM $MgCl_2$. The cultures were grown to an OD_{600} of 1.2 at 37 ^{o}C before induction with 0.5 mM isopropyl-1-thio-β-D-galactopyranoside (IPTG) for 16 h at 30 ^{o}C. Cells were harvested by centrifugation at 4,500 g and the resulting cell paste was stored at -20 ^{o}C until further use.

Frozen cells were thawed on ice and resuspended in Buffer A (25 mM Tris pH 7.5, 1 mM EDTA, 7 mM β-Me, 0.01 % NP-40) containing 100 mM NaCl and 1 mM of the protease inhibitor, phenylmethylsulfonyl fluoride (PMSF). The cell suspension was lysed by three passages through a French press at 15,000 psi. The lysate was then clarified by centrifugation at 20,000 rpm at 4 ^{o}C for 30 min. PCNA was then purified to near homogeneity as previously described, with modifications (47).

In brief, the supernatant was loaded onto two 5 mL HiTrap Q HP columns (GE Healthcare Life Sciences) pre-equilibrated with Buffer A containing 10 % Buffer B (25 mM Tris pH 7.5, 1 mM EDTA, 7 mM β-Me, 0.01 % NP-40, 1 M NaCl) for anion exchange chromatography. The protein was eluted off of the columns using a gradient of Buffer B. Fractions containing PCNA were pooled and diluted with Buffer C (50 mM NaAc pH 5.5, 10 % glycerol, 7 mM β-Me, 0.01 % NP-40) until the approximate NaCl concentration was 50 mM. This sample was applied to two 5 mL HiTrap Heparin HP columns and eluted with

a gradient of Buffer D (50 mM NaAc pH 5.5, 10 % glycerol, 7 mM β-Me, 0.01 % NP-40, 1 M NaCl). The fractions containing the protein was pooled and dialyzed against Buffer E (25 mM KH_2PO_4/K_2HPO_4 pH 7.0, 10 % glycerol, 1 mM DTT) overnight. The sample was then loaded onto a packed 12 mL CHT ceramic hydroxyapatite Type I column. The protein was eluted off of the column using a gradient of Buffer F (300 mM KH_2PO_4/K_2HPO_4 pH 7.0, 10 % glycerol, 1 mM DTT). Fractions containing the protein of interest were pooled and concentrated and subjected to size exclusion chromatography on a SuperdexS200 10/300 GL equilibrated with Buffer G (25 mM Tris pH 7.5, 150 mM NaCl, 10 % Glycerol, 1 mM EDTA, 1 mM DTT).

2.2.2 Expression and purification of recombinant proteins

All plasmids constructed with the pMCSG9 and pMCSG10 vectors (Table 3) were transformed into competent *E. coli* BL21(DE3) cells following standard protocols (48). The same procedure was applied to all of the plasmids.

Single colonies were picked following transformation and grown as 5 mL cultures overnight in LB media overnight supplemented with 100 μg/mL of ampicillin. These cultures were then added to 1 L of the same media and grown to an OD_{600} of 0.8 at 37 ^oC before being induced with 0.5 mM of IPTG for 16 hours at 16 ^oC. Cells were harvested by centrifugation at 4,500 g and the resulting cell paste was stored at -20 ^oC until required for further use.

The frozen cell paste was thawed on ice and the cells were resuspended in HIS Buffer A (25 mM Tris pH 7.5, 500 mM NaCl, 1 mM EDTA, 7 mM β-Me) spiked with 1mM of the protease inhibitor, PMSF. The cell suspension was lysed by two passages

through an Emulsiflex cell homogenizer (Avestin) at 15,000 psi. The lysate was then clarified by centrifugation at 20,000 rpm at 4 ^{o}C for 30 min.

2.2.3 Purification of GST-p21, GST-ATAD5_PIP, GST-ATAD5_PIPM, and GST-ATAD_SIM

Recombinant proteins were purified by immobilized metal affinity chromatography (IMAC) followed by anion exchange chromatography following the manufacturer's suggested protocols. Briefly, clarified lysate was loaded onto two 5 mL prepacked cOmplete His-tag purification columns (Roche) pre-equilibrated with HIS Buffer A and washed with HIS Buffer A + 10 mM imidazole. Proteins were then eluted using HIS Buffer B (25 mM Tris pH 7.5, 500 mM NaCl, 300 mM imidazole, 1 mM EDTA, 7 mM β-Me). The eluents were diluted with Q Buffer A (25 mM Tris pH 7.5, 1 mM EDTA, 7 mM β-Me) until the approximate NaCl concentration was 50mM and applied to two 5mL HiTrap Q HP columns equilibrated with 5% Q Buffer B (25 mM Tris pH 7.5, 1 mM EDTA, 7 mM β-Me, 1 M NaCl) and eluted with a gradient of Q Buffer B. The proteins were then concentrated using centrifugation using Vivaspin 6 ultrafiltration devices with appropriate molecular weight cut offs. The concentrated proteins were stored at -20 ^{o}C after spiking the samples with glycerol to 50 %.

2.2.4 Purification of GST, UAF1_SLD2, UAF1_SLD2M, and ATAD5_SIM

The purification of GST, UAF1_SLD2, UAF1_SLD2M, and ATAD5_SIM proteins followed the above protocol with slight modifications. After IMAC, His-tagged TEV protease was added to GST-ATAD5_SIM, MBP-UAF1_SLD2, and MBP-

UAF1_SLD2M at a 1:20 ratio and dialyzed against 5% Q Buffer B overnight to cleave the GST and MBP tags. Each of the resulting samples were passed through two 5 mL prepacked cOmplete His-tag purification columns (Roche) pre-equilibrated with HIS Buffer A, removing the TEV protease and the His-tagged tags from the flow through. The flow through fraction containing the cleaved protein was then diluted with Q Buffer A to a NaCl concentration of approximately 50 mM and anion exchange chromatography was performed as described above.

The remaining protein on the IMAC column was eluted with HIS Buffer B and these fractions were applied to the appropriate prepacked columns (either MBPTrap HP columns or GSTrap HP columns (GE Healthcare)) equilibrated with HIS Buffer A to remove TEV Protease. Proteins were eluted with the appropriate buffers (GST Elution Buffer (25 mM Tris pH 7.5, 200 mM NaCl, 1 mM EDTA, 7 mM β-Me, 10 mM reduced glutathione) or MBP Elution Buffer (25 mM Tris pH 7.5, 200 mM NaCl, 1 mM EDTA, 7 mM β-Me, 10 mM maltose)). The buffer was exchanged and the proteins were concentrated using centrifugation using Vivaspin 6 ultrafiltration devices with appropriate molecular weight cut offs. The concentrated proteins were stored at -20 ^{o}C after glycerol was added to a final concentration of 50 %.

2.3 Affinity pull-down

GST pull-down and His-affinity pull-downs were carried out using similar protocols. 50 μg of GST-tagged protein (bait) was immobilized onto glutathione sepharose resin equilibrated in Pull-Down Buffer (25 mM HEPES pH 7.5, 150 mM NaCl, 1 mM EDTA, 5 mM β-Me). After 1 hour on ice with gentle agitation, the beads were spun down

by centrifugation (1 minute at 600 g) and the supernatant was removed. The beads were then washed with Pull-Down Buffer to remove excess protein. Prey proteins were then added in excess and allowed to incubate with the immobilized bait for 1 hour on ice with occasional agitation. Unbound protein was then removed through three washes. Each wash involved adding 200 μL of Pull-down buffer, agitating the mixture, spinning down the resin, and removing the supernatant. Finally, bound proteins were stripped from the resin by adding 50 μL of 1x SDS-PAGE loading buffer and boiled for 5 minutes. The samples were then subjected to analysis by SDS-PAGE. The proteins were visualized by Coomassie Brilliant Blue staining.

2.4 Isothermal titration calorimetry

A synthetic 18 amino acid peptide containing ATAD5's PIP box was purchased from and purified by the Tufts University Protein Core Faculty (Boston, USA). The sequence of the peptide was: APPLPSNILDYFRKTSPT. The peptide was then dissolved in ITC buffer (25 mM HEPES pH 7.5, 150 mM NaCl, 5 mM β-Me). The proteins were thoroughly dialyzed and degassed under vacuum before the experiments were conducted. Isothermal titration calorimetry (ITC) measurements were either performed on the VP-ITC calorimeter (GE Healthcare) or the Nano ITC calorimeter (TA Instruments) at 25 ^{o}C. The titration of the peptide into PCNA was performed using the VP-ITC calorimeter. The peptide (750 μM) was loaded into the syringe and injected into the cell containing 50 μM PCNA in 60 injections of 5μL. A control experiment was performed by injecting the peptide into buffer under the same experimental conditions. Experimental traces were

corrected by subtracting the control measurements, and analyzed using Origin 7 (MicroCal). Binding constants, ΔG, and ΔH were calculated

The titrations of ATAD5_SIM into UAF1_SLD2 and UAF1_SLD2M were performed using the Nano ITC calorimeter. ATAD5_SIM (1 mM) was titrated into a cell containing 100 μM of UAF1_SLD2 in 25 2 μL injections following an initial 0.5 μL injection. Control experiments were performed by injecting the peptide into buffer under the same experimental conditions. Experimental traces were corrected by subtracting the control measurements, and analyzed using NanoAnalyze (TA Instruments). Binding constants, ΔG, and ΔH were calculated by fitting the integrated titration data to an independent binding model.

2.4 Yeast two-hybrid assays

The yeast strain used was PJ69-4A and has the genotypes as described (49). Human PCNA was recombinantly expressed with the binding domain of the GAL4 by the integrative vector pASI. Native and mutant N-terminal ATAD5 containing the PIP-box was recombinantly expressed with the activating domain of GAL4 using the pACT2 vector. Yeast cells were sequentially transformed using the LiAc method (50) with the bait plasmid and then the prey plasmid. Selection of the cells containing both the bait and prey plasmids was carried out on media lacking tryptophan and leucine. Positive interactions were scored by growth on medium lacking histidine or histidine and adenine.

2.5 Crystallization

2.5.1 Crystal screening and optimization

Proteins used for crystallization condition screening were either freshly purified or subjected to size exclusion chromatography. Flash-frozen protein stored at -80 ^{o}C was thawed and loaded onto a SuperdexS200 10/300 GL equilibrated with ITC Buffer. Eluted protein was then diluted or concentrated for use in crystallization experiments.

Protein complexes were made prior to setting up crystallization trials. PCNA at a concentration of 1 mg/ml was mixed with 2 molar excess of the synthetic peptide derived from ATAD5 used in ITC experiments. The protein solution was then left to incubate for 1 hour at room temperature before being concentrated to 6 mg/mL. The ATAD_SIM-UAF1_SLD2 complex was collected after ITC experiments were performed and was concentrated to a concentration of 9 mg/mL. The approximate ratio of ATAD5_SIM to UAF1_SLD2 is 3:1.

Crystal screening was carried out using both the hanging drop and sitting drop vapour diffusion method with various commercially available and in-house crystallization kits. The kits used to screen both complexes included: Hampton Research: Crystal Screen kit 1, Crystal Screen kit 2, Natrix, and PEG/Ion Kit and Wizard Classic Crystallization Screen Kit 1, 2, 3, and 4. In addition to the kits mentioned, the peptide-PCNA complex was also screened with: JSGC+ Crystal Screen, Molecular Dimensions: Midas Crystal Screen Kit and in-house PEG/Ion screens with varying PEG molecular weights. 1 μL of protein complex was mixed with 1 μL of the well solution and incubated over a reservoir of the same well solution.

After hits were observed, optimization of crystallization conditions was carried out. Crystals were grown at varying precipitant concentrations and microseeding was employed in order to improve the shape of crystals. A seed solution was prepared by bead-beating harvested crystals suspended in mother liquor and added to fresh drops. Additives were also screened using Hampton Research: Optimization Screen Kit, following the manufacturer's suggested protocol.

2.5.2 Data collection and refinement

Crystals were initially screened at the home-source to identify highly diffracting crystals for data collection. Several crystals were frozen in liquid nitrogen during the screening process. Highly diffracting crystals were sent to the Canadian Light Source (Saskatchewan, Canada) for data collection at the CMCF-081D beam line.

The crystal structure was solved using iMOSFLM (51) and the CCP4 program suite (52). The reflection images were integrated using iMOSFLM and scaled using SCALA and CTRUNCATE (53, 54). Initial phases were obtained by molecular replacement using 3VKK as a search model in PHASER (55). An initial rigid body refinement was carried out by RefMac (56) followed by successive rounds of structure building with COOT (57) and restrained refinements using RefMac. Non-crystallographic symmetry was applied throughout the refinement process.

CHAPTER 3: RESULTS I INTERACTION BETWEEN ATAD5 AND PCNA

3.1 Cloning of plasmids

A variety of plasmids were generated in this study to assess the interactions between ATAD5, PCNA, and UAF1. A summary of the plasmids used and generated is presented in Tables 2 and 3. All of the plasmids used were confirmed to be correct using DNA sequencing.

Subcloning was used to generate the plasmids for the yeast two-hybrid studies. Insert DNA was amplified by PCR and digested with the appropriate restriction endonucleases and ligated into either pASI or pACT2. The pASI and pACT2 vectors encode for fusion proteins between the protein of interest and the binding domain and activating domain of Gal4 respectively.

PIPE cloning was used to generate the plasmids for expression and purification of ATAD5's SIM and UAF1's second SLD (SLD2). The primers used to amplify the insert (by PCR) added a sequence of nucleotides on each end, complementary to the ends on the vector. This technique uses the cell's DNA repair machinery to ligate the plasmid. The plasmids pMCSG9 and pMCSG10 encode the protein of interest fused to the C-terminal of MBP and GST respectfully. MBP and GST are both tagged with an N-terminal poly-His tag and contain a TEV cut site at the C-terminal.

The mutation made to the plasmids containing ATAD's PIP box motif and UAF1's SLD2 was achieved by overlap extension PCR. The key PIP box motifs of ATAD5 (I62, Y65 and F66) were all mutated to Ala using the primers indicated in Table 2. Yang et al. (2011) reported that a K595E mutation in UAF1 would significantly reduce the ability of

UAF1 to bind to ATAD5, so this mutation was also used in this study using the primers indicated in Table 3 (43).

3.2 Purification of proteins

3.2.1 Purification of PCNA

Human PCNA was expressed in *E. coli* and purified to near homogeneity (Figure 6). Following cell lysis, the sample was clarified using high-speed centrifugation for 15 min at 7000 g. The supernatant was then applied onto prepacked HiTrap Q columns for anion exchange chromatography (Figure 6A). The protein was eluted from the column using an increasing gradient of ionic strength. The protein was further purified by heparin affinity chromatography (Figure 6B). The fractions containing PCNA from anion exchange chromatography was diluted to reduce the concentration of NaCl before being loaded onto HiTrap Heparin columns. The protein was again eluted from the column using a gradient of increasing ionic strength. PCNA was still not sufficiently pure, so the sample was subjected to mix mode chromatography via ceramic hydroxyapatite (Figure 6C). Hydroxyapatite chromatography has unique separation properties and can sometimes separate proteins shown as homogeneous by other chromatographic or electrophoretic techniques (58). The sample was applied to a 12 mL column and eluted using an increasing gradient of potassium phosphate. The final low molecular weight contaminants were removed by size exclusion chromatography (Figure 6D), as PCNA is significantly larger in solution (as a trimer). Typically, 5 grams of cell paste yielded 25mg of protein. SDS-PAGE analysis shows that this protein is suitable for biochemical and structural studies.

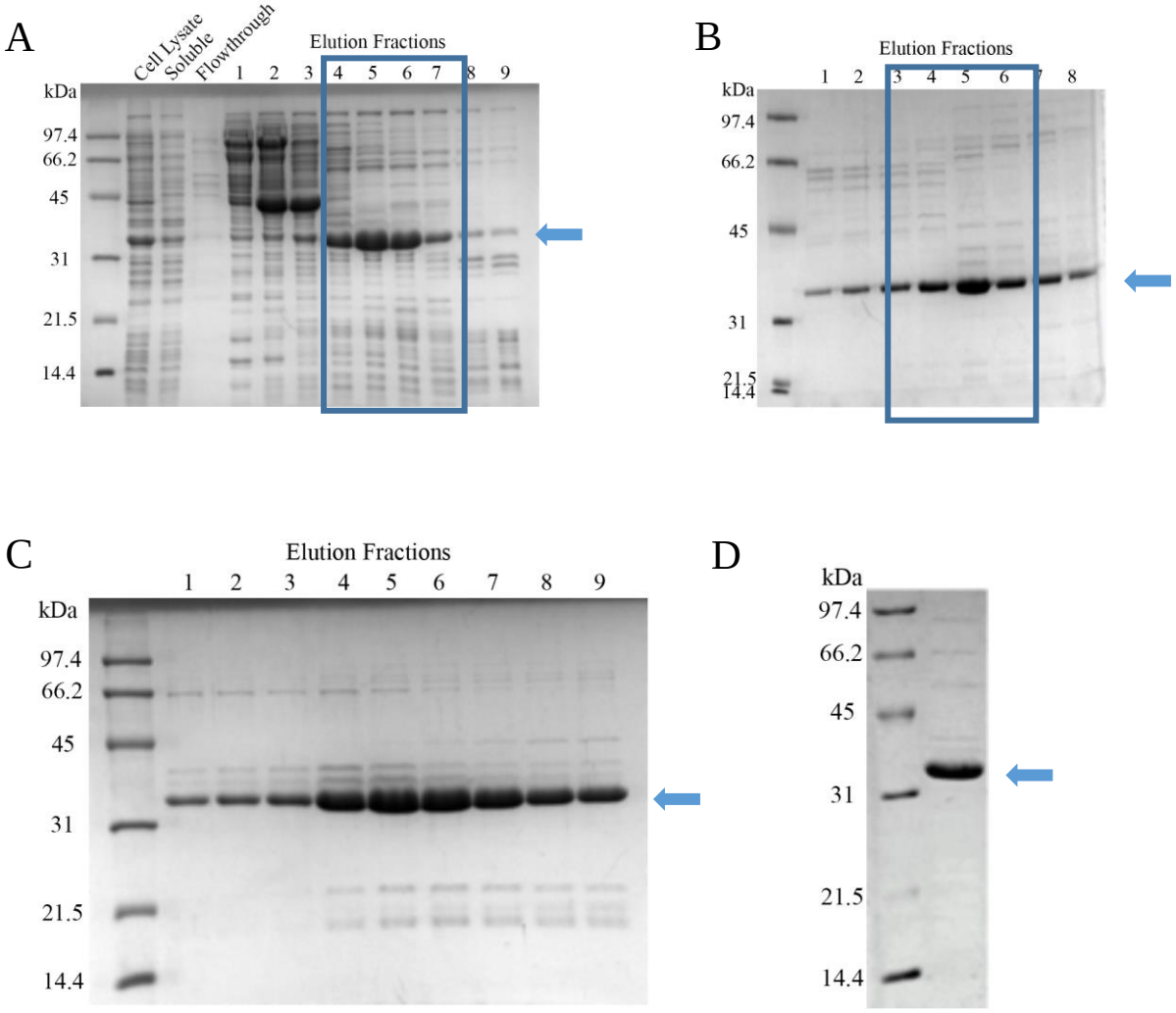

Figure 6. Purification of human proliferating cell nuclear antigen (PCNA) (28.7 kDa). SDS-PAGE analysis after each stage of chromatography. Blue arrows indicate the band of interest. A) Anion exchange chromatography using HiTrap Q columns. Cell lysate, soluble protein, flow-through, and eluted fractions are indicated. Fractions in blue box were pooled. B) Eluted fractions from Heparin affinity chromatography. Fractions 4-6 were pooled. C) Eluted fractions from hydroxyapatite chromatography. D) Peak fraction of PCNA after size exclusion chromatography. PCNA is near homogeneity.

Despite having a predicted molecular weight of 28.7 kDa, individual PCNA monomers runs at about 34-35 kDa on a 15% SDS-PAGE gel. Gulbis et al. 1996 had previously reported that human PCNA runs at a higher apparent molecular weight (47). PCNA from other organisms such as *Schizoscaccharomyces pombe* and tomatoes have also been reported to run higher than their expected molecular weight (59, 60).

3.2.2 Purification of GST-fusion proteins

The GST-fusion proteins (GST-p21, GST-ATAD5_PIP and GST-ATAD5_PIPM) were expressed in *E. coli* following the same growth and induction parameters. The vector (pMCSG10) that encodes the recombinant proteins includes a poly-his tag in the N terminal of GST, allowing IMAC to be utilized as the first purification step. Figure 7A shows a representative purification of GST-ATAD5_PIPM.

The proteins were purified to near homogeneity after IMAC and anion exchange chromatography. All of the proteins were soluble following cell lysis. Clarified lysate was loaded onto 5 mL prepacked cOmplete His-tag purification columns (Roche). After a wash with a low concentration of imidazole, the remaining proteins were eluted using a high concentration of imidazole. The eluted sample was then diluted to reduce the NaCl concentration and loaded onto HiTrap Q HP columns (GE Healthcare) for anion exchange chromatography. The protein was then eluted using an increasing gradient of ionic strength. Typically, 10 mg of protein was obtained from 0.5 L cultures.

A

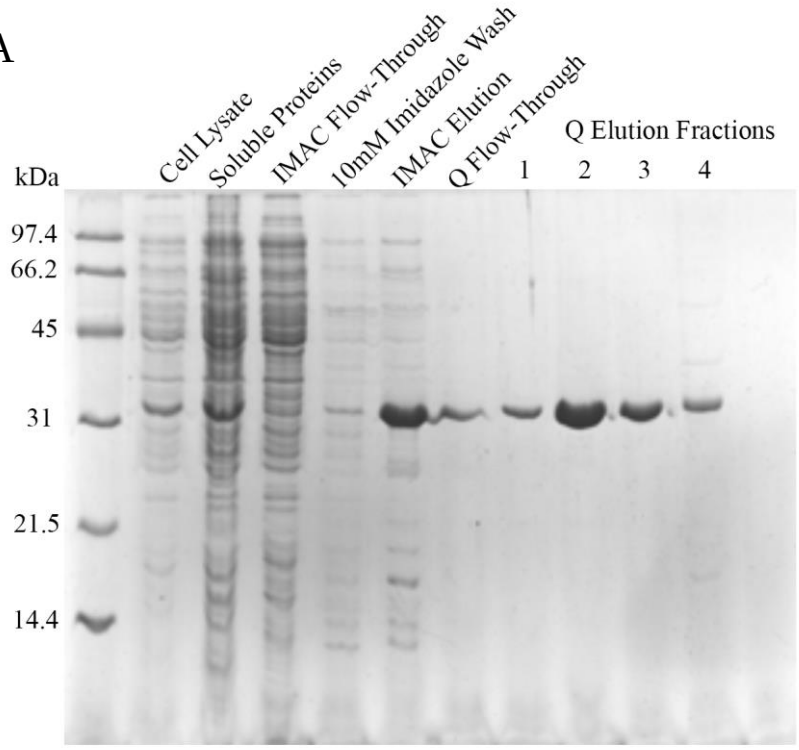
Cell Lysate
Soluble Proteins
IMAC Flow-Through
10mM Imidazole Wash
IMAC Elution
Q Flow-Through
Q Elution Fractions
1
2
3
4
kDa
97.4
66.2
45
31
21.5
14.4

B

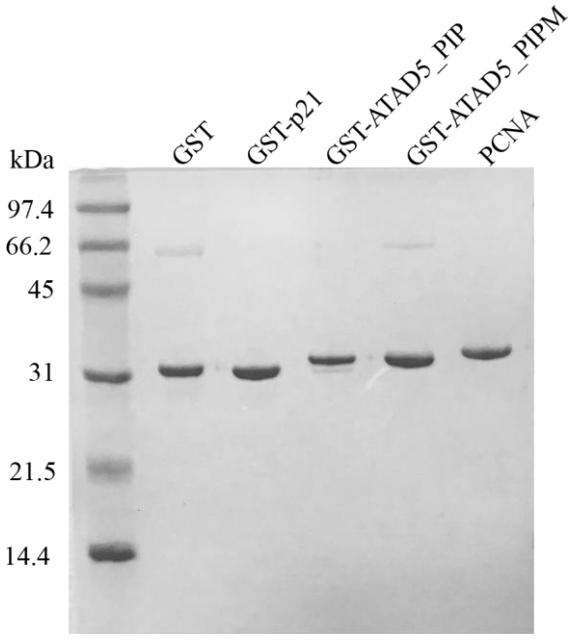
GST
GST-p21
GST-ATAD5_PIP
GST-ATAD5_PIPM
PCNA
kDa
97.4
66.2
45
31
21.5
14.4

Figure 7. Purification of GST-fusion proteins. Purification of ATAD5_PIPM as a representative purification of GST-fusion proteins. A) SDS-PAGE analysis of the cell lysate and soluble fraction. The sample was applied to two cOmplete His-tag purification columns, washed with 10mM imidazole and eluted with 300mM imidazole. Following IMAC, sample was subjected to anion exchange chromatography via HiTrap Q HP column. Protein was eluted using increasing ionic strength. B) SDS-PAGE analysis of all GST and GST-fusion proteins used in pulldowns. GST-p21 (30.4 kDa), GST-ATAD5_PIP (31.2 kDa), and GST-ATAD5_PIPM (31.1 kDa) ran close to their expected molecular weights. The apparent molecular weight of GST (28.3 kDa) and PCNA (28.7 kDa) were slightly higher than expected.

The GST protein to be used as negative controls for the affinity pull-downs were purified from the cleavage products of tagged protein with TEV protease. Both the GST and TEV protease contained the poly-His tag, so GST affinity chromatography was used to separate them. GST and TEV protease was eluted from the IMAC columns after the cleaved protein of interest was removed. The sample was directly loaded onto a GSTrap HP (GE Healthcare) and eluted with a buffer containing 10 mM of reduced glutathione. Typically, 5 mg of GST was obtained from the digestion of 7 mg of GST-p21.

These proteins were resolved close to their predicted molecular weights during SDS-PAGE analysis and are of sufficient quality to be used in biochemical assays (Figure 7B). GST-p21 (30.4 kDa), GST-ATAD5_PIP (31.2 kDa), and GST-ATAD5_PIPM (31.3 kDa) ran close to their expected molecular weights. The apparent molecular weight of GST (28.3 kDa) was slightly higher than expected.

3.2 GST Pull-down assays

Work by a previous student showed that the identified putative PIP box in ATAD5's N-terminal was able to bind to PCNA, and that mutation of these residues abolished the binding. The GST pull-down assay was replicated to confirm the findings. In brief, GST-bound proteins (bait) were incubated with glutathione agarose resin and allowed to bind. Unbound protein was then washed off and PCNA (prey) was added to the resin in excess. After several rounds of washing, only the protein that interacts with the bait remain. These proteins were eluted from the resin and analyzed using SDS-PAGE on a 15% polyacrylamide gel (Figure 8).

	INPUT				OUTPUT			
PCNA	+	+	+	+	+	+	+	+
GST	+	-	-	-	+	-	-	-
GST-P21	-	+	-	-	-	+	-	-
GST-ATAD5_PIP	-	-	+	-	-	-	+	-
GST-ATAD5_PIPM	-	-	-	+	-	-	-	+

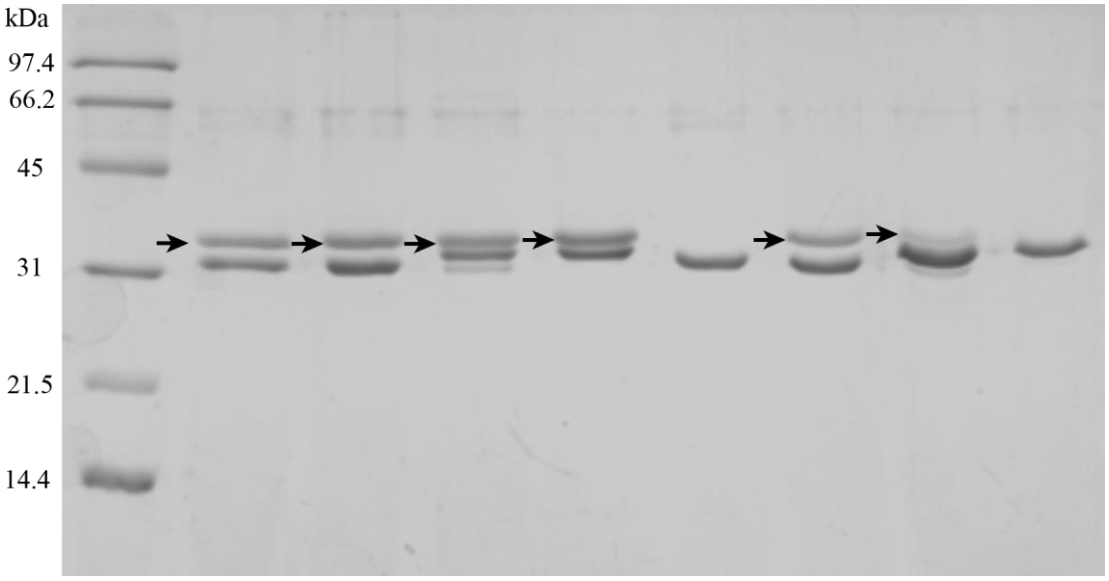

Figure 8. Pull-down assay showing the interaction between ATAD's PIP box and PCNA. Excess GST or GST-fused protein was immobilized onto glutathione resin. Unbound protein was then washed off and PCNA (prey) was added to the resin in 2 molar excess. After several rounds of washing, bound protein were eluted from the resin and analyzed by SDS-PAGE on a 15% polyacrylamide gel. Proteins used in each reaction is shown above by a "+", PCNA is indicated by arrows.

PCNA was observed to co-elute with the native ATAD5 PIP box along with the positive control using the PIP box from p21. The intensity of the PCNA band was significantly lower in the lane containing ATAD5 compared to the lane containing p21. This suggests that the interaction between the PIP box of ATAD5 is weaker than that of P21 with PCNA. Mutation of the two aromatic residues (Tyr65 and Phe66) to Ala abolishes the interaction, as PCNA not present in the eluted proteins (Figure 7).

From the Pull-down experiment, we can conclude that the putative PIP box from ATAD5 interacts with PCNA. Also, this experiment demonstrates that the two aromatic residues of this PIP box is important for binding. Therefore, we can infer that the binding mode of this PIP box to PCNA is similar to that of canonical PIP boxes.

3.3 Yeast two-hybrid assays

To confirm the results of the GST pull-down assays, the interaction between the N-terminal of ATAD5 containing the PIP box with PCNA was analyzed in a yeast two-hybrid system. The two-hybrid system takes advantage of a transcriptional activator that has two separable functions: one to bind to a specific region of DNA, and the second, to increase the frequency with which transcription is initiated on an adjacent gene (Figure 9A) (61). The binding domain (BD) and activating domain (AD) of the transcriptional activator Gal4 is encoded separately by the pASI and pACT2 vectors fused to proteins of interest (62). The ability to synthesize Leu and Trp is conferred by pASI and pACT2 respectlvely. The yeast stain that is used in this study (PJ69-4A), will express β-galactosidase and be able to synthesize His and Ade upon activation of the reporter genes by Gal4 (49).

PJ69-4A yeast cells were sequentially transformed with plasmids made from the pASI vector and then the pACT2 vector. PJ69-4A cells were initially transformed using the LiAc/single-stranded carrier DNA/PEG method with plasmids made with the pASI vector and plated on selective media lacking Trp. Colonies were picked for each plasmid and then subsequently transformed with plasmids made with the pACT2 vector. Co-transformed cells were selected by their ability to grow on selective media lacking both Trp and Leu.

Binding of the N-terminal 250 amino acid residues of ATAD5 and PCNA was assessed by spot plating co-transformed cells on increasingly selective media. Transcription of the reporter genes responsible for His and Ade synthesis will allow the cells to survive on media without these amino acid residues. Cells transformed with both pASI-PCNA and pACT2-A250 were able to grow on plates lacking Trp, Leu, and His and/or Ade (Figure 9B). Cells transformed with both pASI-PCNA and pACT2-ATAD_N250M (containing mutations to key PIP box residues), were not able to grow on the plates lacking His and/or Ade (Figure 9B). From these results, we have confirmed that the putative PIP box is able to interact with PCNA and mutations of the conserved residues in the PIP box abolishes binding.

3.4 Isothermal titration calorimetry

With the interaction between ATAD5's PIP box and PCNA confirmed by both GST pull-down assays and the yeast two-hybrid system, we wanted to characterize the interaction. The thermodynamic parameters of the interaction were characterized by ITC using the VP-ITC calorimeter. In ITC, the energy absorbed or given off from a reaction

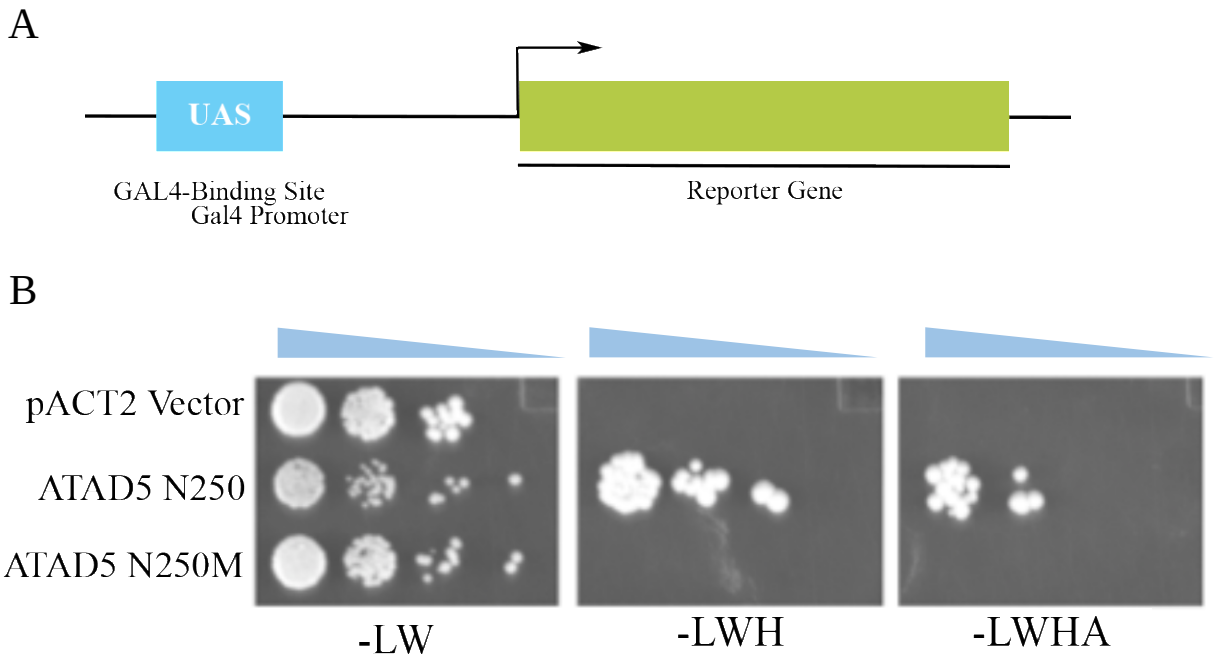

Figure 9. Interaction of ATAD5's N-terminal 250 amino acids with native PCNA in a yeast two-hybrid system. A) Binding of the two proteins fused to Gal4's binding domain and activating domain will start transcription of t. B) PJ694A cells were successively transformed with the plasmid encoding native human PCNA and then with either the pACT2 vector, encoding only the AD of Gal4, and pACT2-ATAD5_N250 or pACT2-ATAD5_N250M which encodes the N terminal 250 amino acids of ATAD5 or the mutant. These cells were then spot plated with an initial dilution of 1000x and then serial diluted 4 times on increasing selective media (blue triangles represent dilution).

between two components is measured and the thermodynamic terms that define the binding affinity, enthalpy (ΔH) and entropy (ΔS), can be determined (63).

The binding affinity of ATAD5's PIP box with PCNA was determined using a synthetic peptide. The full-length ATAD5 protein is relatively large, comprising of 1844 amino acid residues, with the first ~1000 residues predicted to be disordered. For this reason, an 18 amino acid residue peptide was synthesized that contained the PIP box of ATAD5. The flanking sequence of amino acids on both sides of the PIP box were conserved. The synthetic peptide containing the PIP box of ATAD5 was diluted in ITC buffer and thoroughly dialyzed. The pH of the peptide sample after dialysis overnight did not match that of the buffer, so the time of dialysis was extended to 36 hours total. The peptide was loaded into the syringe and titrated stepwise into the cell containing PCNA. A control experiment was conducted in which the peptide was titrated into a cell containing ITC Buffer only (Figure 10A). The control experiment was subtracted from the experimental traces and fitted to a one-site binding model (Figure 10B-C). The K_d of the interaction was determined to be 6.17 ± 0.78 μM with an n of 0.93 ± 0.01. The stoichiometry of the reaction is close to 1, meaning that each peptide binds to one monomer. The ΔH, ΔS and ΔG of the reaction is -2.18 ± 0.04 kcal, 16.5 cal mol^{-1} K^{-1} and -7.01 kcal/mol respectively.

From the ITC data, we determined that the interaction is in the low micromolar range, each monomer of PCNA is able to bind to one peptide, and that the interaction occurs under favourable conditions, however it is non-spontaneous.

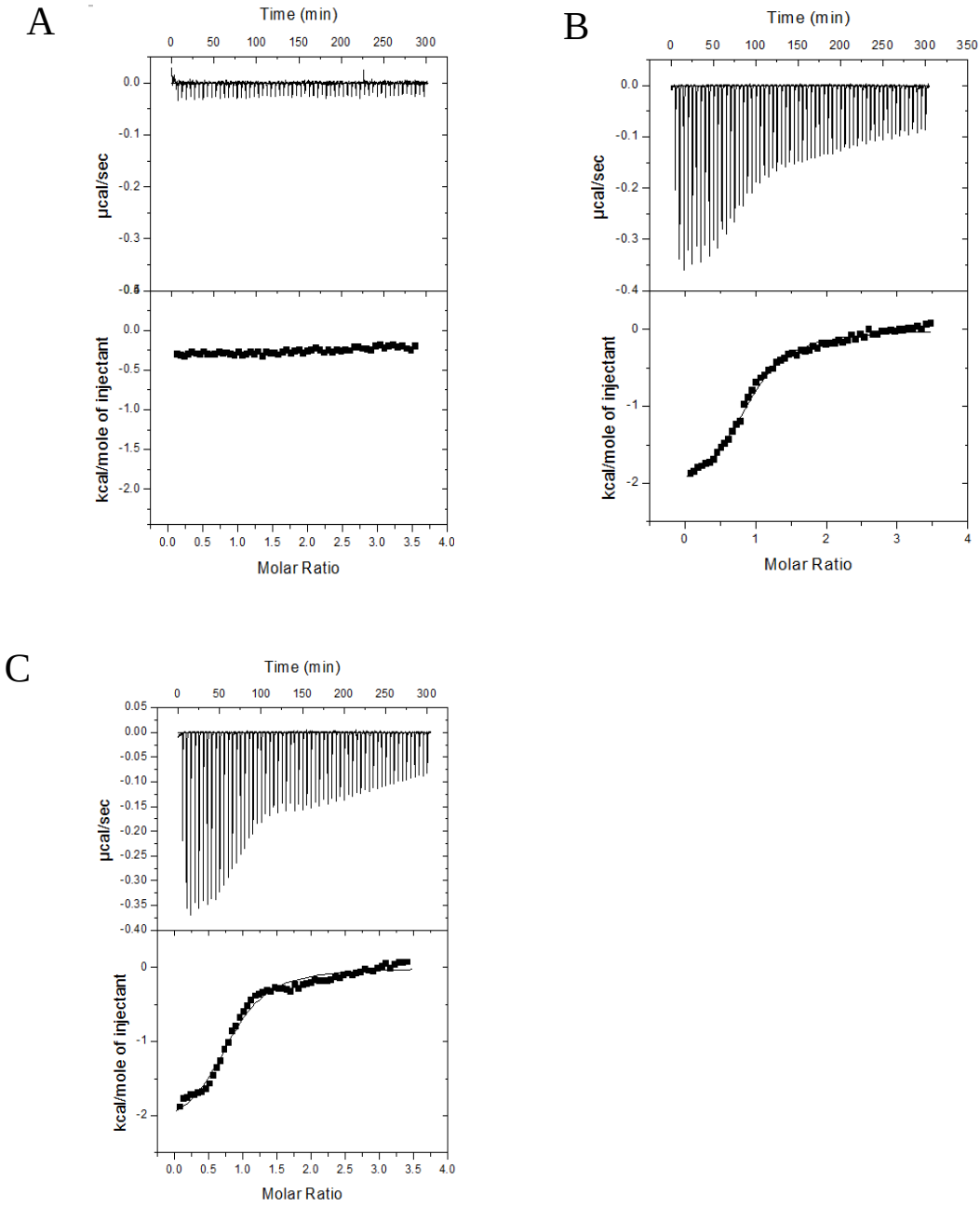

Figure 10. Determination of the thermodynamic parameters of the binding between ATAD5's PIP box and PCNA. Thoroughly dialyzed peptide (800µM) was titrated stepwise into the cell in 2.5µL injections at 25°C. Binding thermograms from titration of a synthetic peptide containing ATAD5's PIP box into the cell. A) A control experiment was conducted in which the peptide was titrated into a cell containing ITC Buffer only. B) The peptide was titrated into a cell containing 40µM of PCNA. C) Replicate of titration described in (B)

3.5 Crystallization of PCNA:ATAD5 peptide complex

In order to determine the structural features of the binding between the PIP box of ATAD5 and PCNA, the x-ray crystal structure was determined. Since ATAD5 is too large for crystallographic experiments, the 18 amino acid residue peptide from ITC experiments was used. Crystallization trials were conducted to determine the condition where both PCNA and the peptide would co-crystalize.

3.5.1 Screening and optimization

Crystallization trials were carried out in order to determine the condition required to crystalize the protein-peptide complex. PCNA at 1 mg/mL was incubated with the peptide dissolved in ITC Buffer in 3 molar excess for 1 hour at room temperature. The protein complex was then concentrated to 6 mg/mL. Both the hanging drop and sitting drop vapour diffusion techniques were used in the screen. 1 μL of the protein complex was mixed with 1 μL of the well solution and suspended over 500 μL resovoir of well solution. The well solutions were from commercial and in-house crystallization kits. In the end over 1000 unique conditions were screened. Many conditions produced crystals, however, they closely resembled the native crystallization conditions and were rejected. Other conditions that were identified by the screen included: 2 M ammonium sulphate, citrate pH 5.5, 50 % PEG 400, 0.1 M sodium acetate/acetic acid pH 4.5, and 30 % PEG 400, 0.2 M calcium acetate (Figure 11). The condition using 30 % PEG 400 and 0.2 M calcium acetate was reproducible and produced crystals within 2-3 days so it was chosen for optimization. Initially, the crystals were not well formed (Figure 11D); however, if PCNA was subjected to size exclusion chromatography on a Sephadex S200 10/300 GL

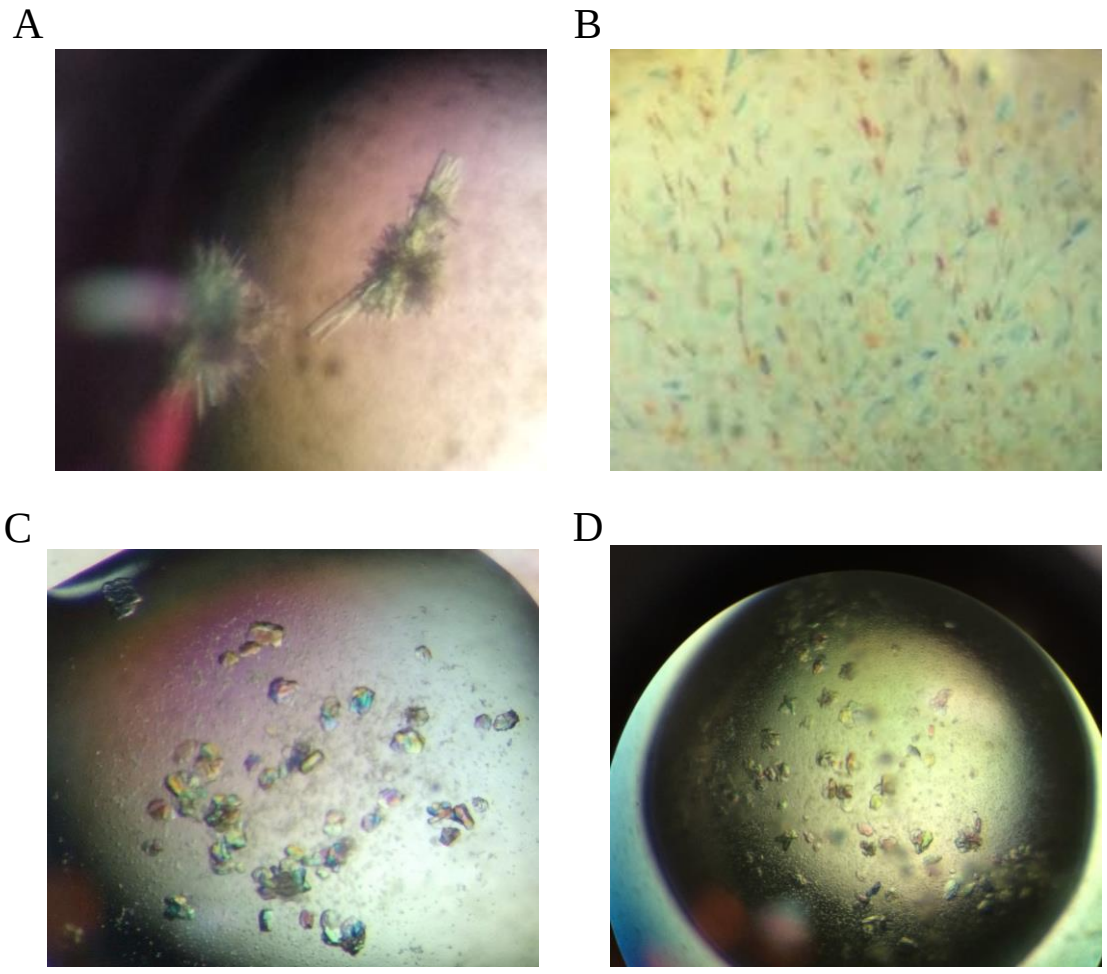

Figure 11. Hits from crystallization trials for complex of PCNA and a synthetic peptide derived from ATAD5. 1 μL of the protein complex was mixed with 1 μL of the well solution and suspended on 500 μL of well solution. The well solutions were from commercial and in-house crystallization kits. 3 hits were observed. A) 2 M ammonium sulfate, citrate pH 5.5. B) 50% PEG 400, 0.1 M sodium acetate/acetic acid pH 4.5. C) 30% PEG 400, 0.2 M calcium acetate. D) Crystallization condition from (C) was reproducible.

column equilibrated with 25 mM HEPES pH 7.5, 150 mM NaCl and 5 mM β-Me prior to forming the complex, more of the resulting crystals are well-shaped and larger (Figure 12A). These crystals did not diffract past 6 Å however.

Both the micro seeding and streak seeding techniques were used in an attempt to produce better diffracting crystals. Microseeding appeared to be more effective, however, large crystal showers were observed (Figure 12B). Different precipitant concentrations were then screened in combination with microseeding. Larger well-shaped crystals were observed at 25 % PEG 400 (Figure 12C). Since low molecular weight PEGs are suitable cryoprotectants, these crystals were directly frozen in liquid nitrogen to be used in x-ray diffraction experiments. Despite lacking any visual imperfections, the crystals only diffracted to a maximum of 4.5 Å at the Canadian Light Source. After multiple rounds of crystallization without high-diffracting crystals, additives were screened from the Optimization Screen Kit (Hampton Research) following the manufacturer's instructions. Many additives produced the same well-shaped crystals, all corresponding to metal cations. The largest, well-shaped crystals appeared with the addition of $MgCl_2$. Finally, a crystal of the protein complex was grown in 25 % PEG 400, 0.2 M calcium acetate, and 10 mM $MgCl_2$ with microseeding (Figure 11D). These crystals diffracted with higher resolution, up to 2.2 Å on the CMCF-081D beam line at the Canadian Light Source.

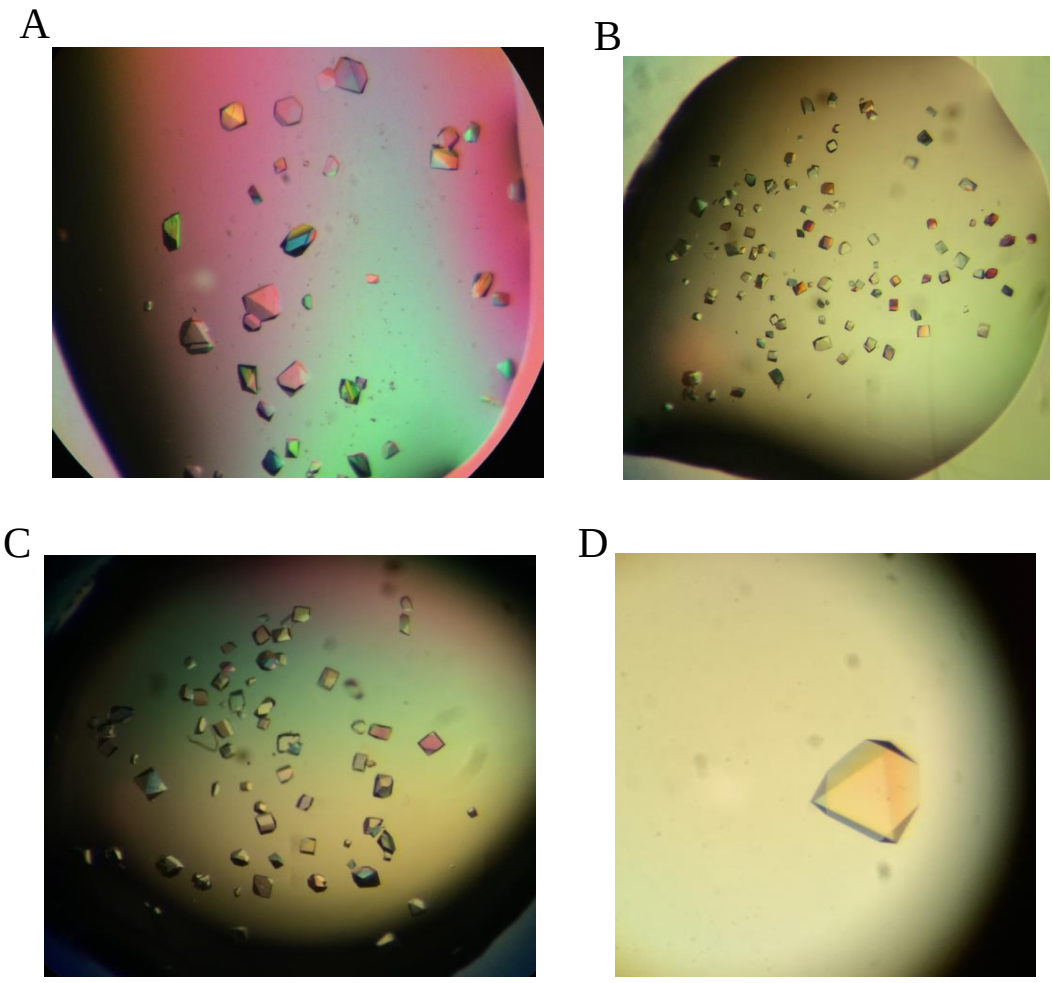

Figure 12. Optimization of the crystallization condition for the crystallization of PCNA/Peptide complex. The initial condition of 30% PEG 400, 0.2M calcium acetate was used. 2 μL of the protein complex was mixed with 2 μL of the well solution and suspended over 500 μL of well solution. A) Use of protein refreshed via size exclusion chromatography pre-equilibrated in ITC Buffer (25 mM HEPES pH 7.5, 150 mM NaCl, 5 mM β-Me) produced larger well shaped crystals. B) Protein crystals from A were used to make a seed stock for microseeding. 0.2 μL of this stock was added to drops. Many small well-formed crystals grew. C) Concentration of PEG 400 was reduced to 25 %. This produced larger crystals, however none of the crystals diffracted past 4.5 Å. D) Final drop was spiked with $MgCl_2$ to a final concentration of 10 mM. Resulting crystals were large and diffracted to high resolution.

3.5.2 Structure determination of PCNA:ATAD5 peptide complex

The highest diffracting dataset was used to solve the structure of the complex between PCNA and the synthetic peptide containing ATAD5's PIP box. First, the collection of refraction images was processed in iMOSFLM (51). From previous datasets obtained from the home source, the space group was thought to be h6, however, the recent high-resolution dataset showed that the space group was either $P3_121$ or $P3_122$. The cell parameters were consistent with the previous low-resolution dataset, with two axis of the same length (a, b = 83.7 Å) and one significantly longer axis (c = 209.6 Å). Integration of the data set was disrupted by refraction images that contained large spots. Removal of these images from the dataset allowed for the integration of the remaining dataset into one .mtz file. The data was then scaled to a resolution of 2.2 Å with CTRUNCATE and SCALA (53). Initial phases were obtained by molecular replacement in PHASER using monomeric human PCNA structure (PDB ID: 3VKX) as a search model (55). Here, the space group was determined to be $P3_121$, with three PCNA monomers in the asymmetric unit cell. After an initial rigid body refinement in RefMac, successive rounds of structure building in COOT and smooth body refinements with non-crystallographic symmetry restraints were carried out (56, 57). Un-modeled blobs around the hydrophobic region of PCNA where initially filled with Ala before mutation of the residues to correspond with the peptide sequence. The data collection and refinement statistics are summarized in Table 4.

Table 4. Data collection and refinement statistics for the structure of PCNA with a synthetic peptide derived from ATAD5.*

Data collection	
Space group	$P3_121$
Cell dimensions□ □	
a, *b*, *c* (Å)	83.7, 83.7, 209.6
α, β, γ (°)	90, 90, 120
Resolution (Å)	50.0-2.20(2.32-2.20)
R_{sym} or R_{merge}	0.10(0.63)
$I/\sigma I$	10.9 (3.4)
Completeness (%)	99.9 (100.0)
Redundancy	8.5 (8.9)
Refinement	
Resolution (Å)	50.0-2.20
No. reflections	44, 086
$R_{work/}$ R_{free}	22.5/27.6
No. atoms	
Protein	5852
Peptide	289
Mg^{2+}/PEG	2/14
Water	228
B-factors	
Protein	45.8
Peptide	66.1
Mg^{2+}/PEG	58.9/47.5
Water	45.9
R.m.s deviations	
Bond lengths (Å)	0.010
Bond angles (º)	1.53

*Values in parenthesis are for the highest-resolution shell. Crystal data was collected on the CMCF-081D beam line at the Canadian Light Source (Saskatchewan, ON). The data was integrated using iMOSFLM and scaled with SCALA and CTRUNCATE. Molecular replacement was performed using PHASER with the search model 3VKX. Successive rounds of refinement and model building was done using REFMAC and Coot.

3.5.3 PCNA:ATAD5 peptide complex structure

The crystal structure was solved by molecular replacement to a resolution of 2.20 Å. The PCNA structure has three subunits that are arranged head-to-tail (Figure 13C). The quaternary structure is of a toroid, as N- and C-terminal regions form subunit-subunit contacts. The monomers are structurally similar, with RMSD values between subunits ranging from 0.397 to 0.559 Å over 248 residues and surface areas ranging from 12318 to 12737 $Å^2$. The PCNA trimer has a pseudo 6-fold symmetry, with two similar domains in each subunit. Each domain consists of 2 α-helices and 9 β-strands. The trimer therefore consists of 12 α-helices and 54 β-strands in total. Each monomer was modelled unambiguously from residues 1-256, however there was poor density for the five C-terminal residues and a loop region in two of the monomers. Similar regions of missing density have been reported in other PCNA structures as well (64–66).

One peptide molecule binds to each of the three PCNA monomers in the asymmetric unit. Binding the peptide does require or induce large-scale structural rearrangements of PCNA as there is little global change upon peptide binding (Figure 14). The peptide-bound PCNA structure is structurally similar to the apo PCNA structure (1VYM), with a RMSD of 0.75Å over 248 residues. According to the x-ray structure model, 9 to 13 of the 18 amino acids in the peptide were resolved in each subunit.

The three peptides are also structurally similar, with RMSD values between 0.37 to 0.51 Å over 66 atoms. The surface areas of the peptide range from 1395 to 1729 $Å^2$ with the contact surface area ranging from 562 to 673 $Å^2$ (approximately 40 %). Figure 13D shows the electron density ($2F_o - F_c$) map contoured to 1.2 Å around the peptide with respect to PCNA.

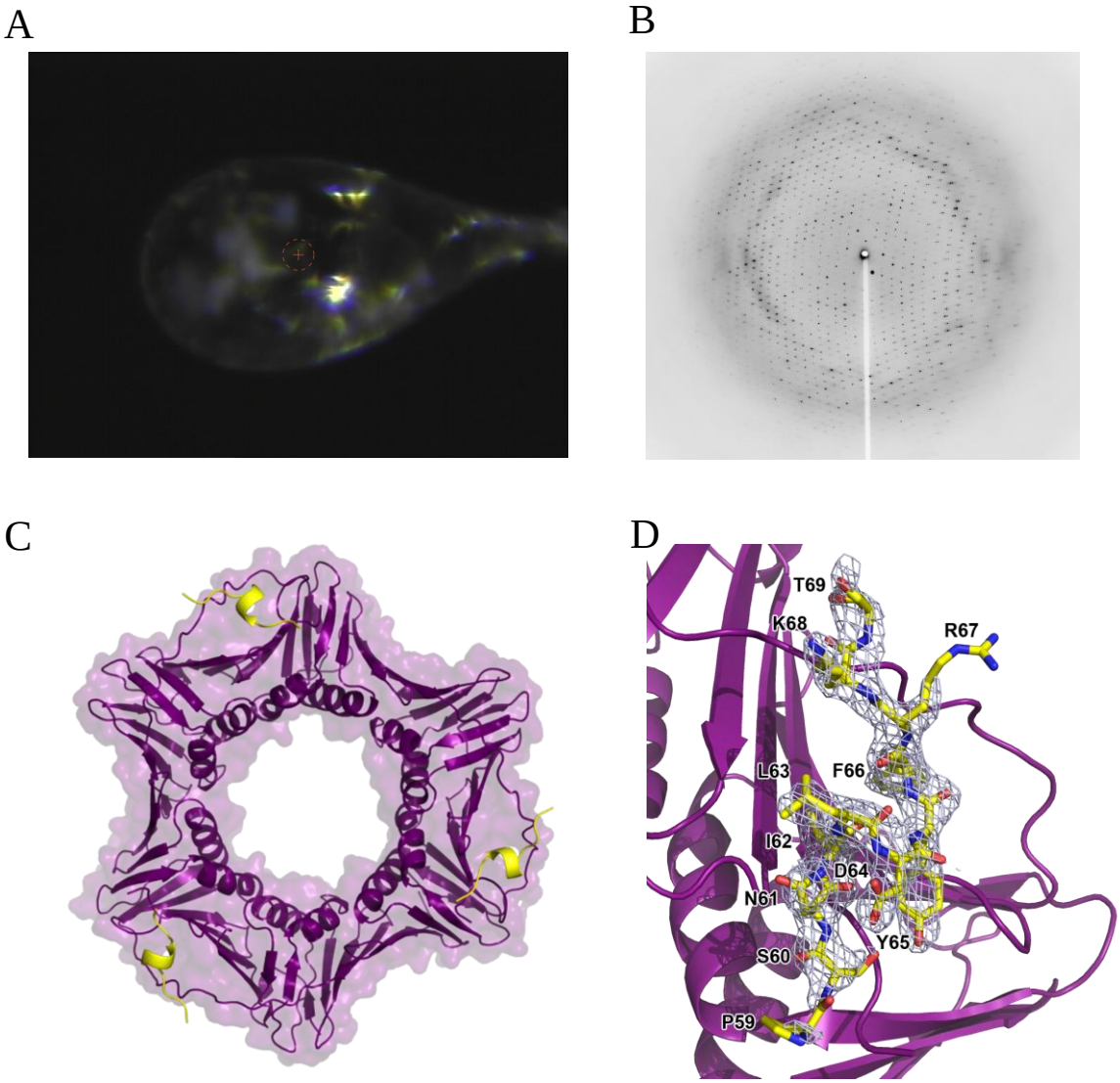

Figure 13. Structure of PCNA co-crystalized with a synthetic peptide derived from ATAD5. A) Crystal mounted onto 0.2-0.3mm loop and directly frozen in liquid nitrogen. B) Diffraction image taken of crystal at CMCF-081D beam line at the Canadian Light Source. Crystals diffracted to 2.2Å and belonged to the space group $P3_121$ with unit cell dimensions of *a, b* = 83.7 Å and *c* = 209.6 Å. C) Cartoon representation of complex structure with transparent surface. One peptide (yellow) binds to each monomer of PCNA (purple). D) 11-13 residues of the peptide were resolved in the final structure. $2F_o - F_c$ map of peptide represented as sticks (yellow) is shown and contoured to 1.2 Å.

Figure 14. Binding of peptide does not induce significant conformational changes in PCNA. Cartoon representation of the two structures superimposed is shown. The co-crystal structure of PCNA with the ATAD5 peptide (purple) has a high global similarity to the apo form of PCNA (grey; PDB ID: 1VYM) when superimposed with a RMSD 0.75Å over 248 residues.

The binding of the peptide containing ATAD5'S PIP box to PCNA is topologically conserved with respect to proteins with canonical PIP boxes (65, 67–70). There are two main interacting regions on the peptide. The first is the PIP box region which forms a 3_{10} α-helix with the hydrophobic residue pointing towards the minor hydrophobic groove of PCNA and the two aromatic residues pointing towards the major hydrophobic pocket (Figure 15A). The second is near the C-terminal region where Arg 67 and Thr 69 form hydrogen bonds with Gln 125 and Gly 127 of the IDCL (Figure 15B). The C-terminal of the peptide points toward the bulk solvent however, instead of interacting with amino acid residues along the IDCL.

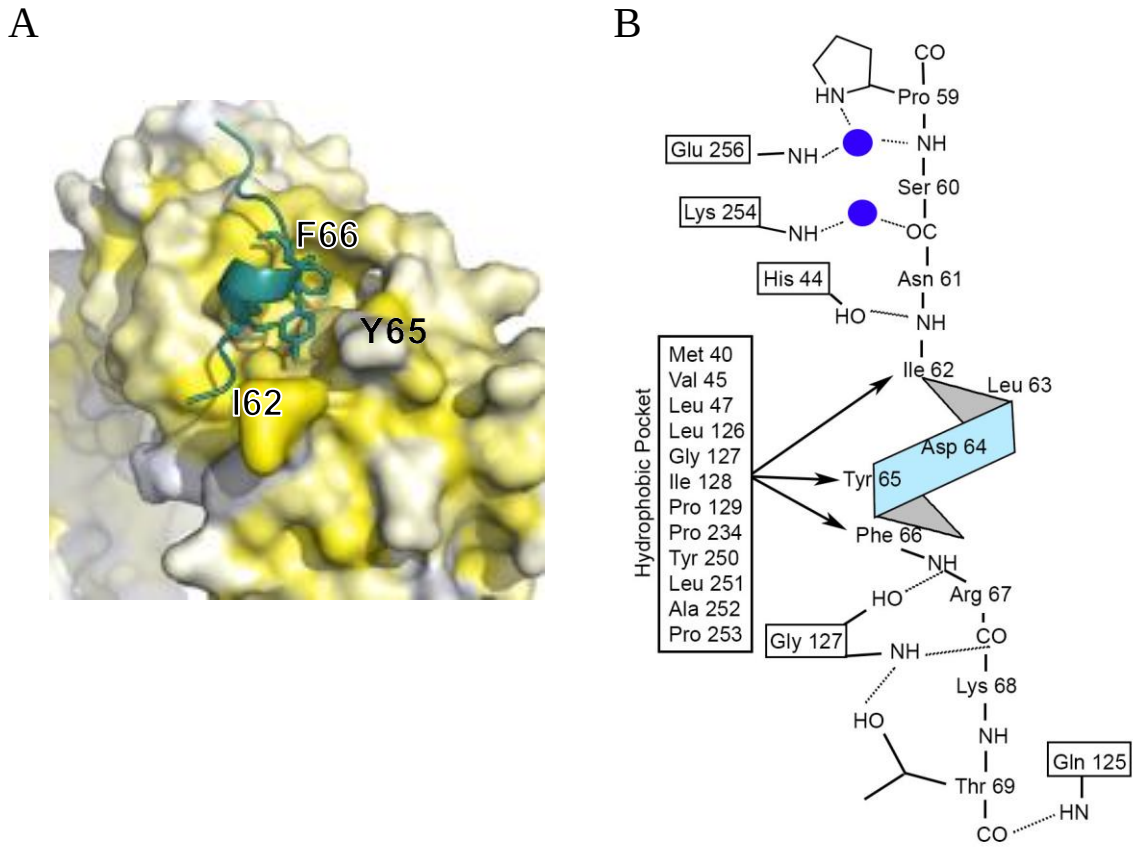

Figure 15. ATAD5 binds to the hydrophobic pocket of PCNA. A) Surface representation of PCNA with hydrophobic areas coloured yellow and the peptide (teal) represented as ribbon. PIP box residues are represented as sticks. The side chains of Ile 62 faces the minor hydrophobic groove and the side chains of Tyr 65 and Phe 66 point toward the major hydrophobic pocket. B) Scheme of interactions between the synthetic peptide derived from ATAD5 and PCNA. Indicated are the residues (framed for PCNA), bound water (blue circles, hydrogen bonds (dotted lines), and non-bonded interactions (black arrows). The helix is shaded light blue.

CHAPTER 4: RESULTS II UAF1-ATAD5 INTERACTION

After characterizing the interaction between ATAD5's PIP box and PCNA, we wanted to explore ATAD5's interactions with UAF1. ATAD5 contains a SIM which is thought to interact with a SLD on the C-terminal of UAF1. In order to study this interaction, the genes encoding the domains of interest from the appropriate proteins were cloned into expression vectors. A mutation (K595E) was made to UAF1's SLD that has been previously shown to reduce its binding to ATAD5. These proteins were then subsequently expressed and used for biochemical characterization.

4.1 Expression and purification of ATAD5_SIM, UAF1_SLD2 and UAF1_SLD2M

ATAD5_SIM, UAF1_SLD2 and UAF1_SLD2M were expressed in *E. coli* following the same growth and induction parameters. pMCSG10 encodes a N-terminally fused MBP tag to the protein of interest with a TEV cut site in between. The MBP tag contains a poly-his tag at its N-terminal allowing IMAC to be used in the purification of the protein of interest.

All of the proteins were soluble and purified to near homogeneity after two rounds of IMAC and anion exchange chromatography. The purification of UAF1_SLD2 is shown in figure 16A-C as a representative purification. Clarified lysate was subjected to IMAC using 5 mL prepacked cOmplete His-tag purification columns (Roche). Following elution, TEV protease was added to the sample at a 1:40 ratio and the sample was left to dialyze overnight in buffer suitable for TEV protease activity (25 mM Tris pH 7.5, 150 mM NaCl, 0.5 mM EDTA, 7 mM β-Me). The sample was then passed through the cOmplete His-tag purification columns (Roche), untagged proteins flowed through the column, leaving the His-tagged TEV protease and MBP behind. The flow-through sample was then diluted

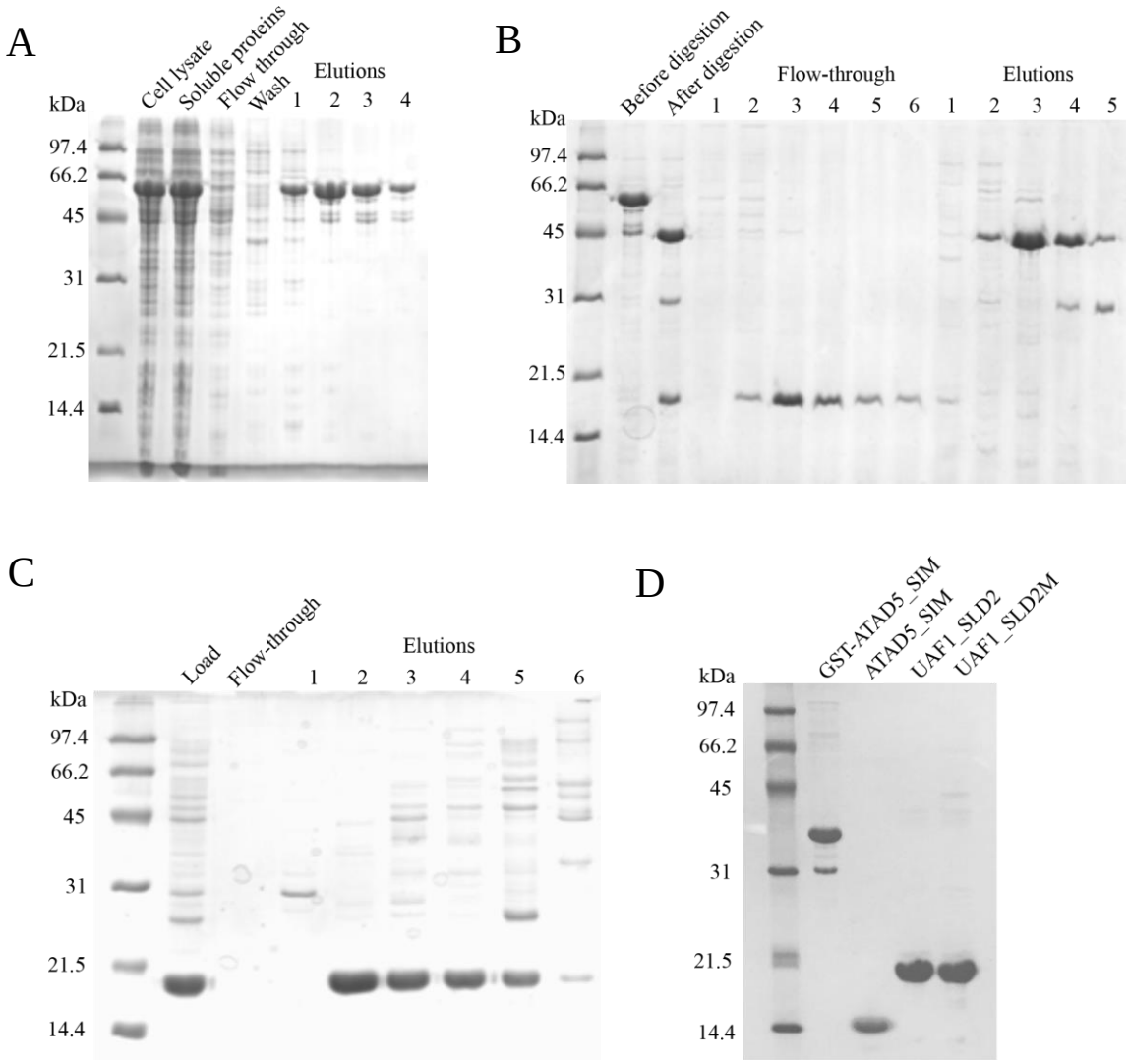

Figure 16. Representative purification of tagged protein and subsequent tag cleavage by TEV protease. UAF1_SLD was expressed in *e. coli* as a MBP-fusion protein. A) SDS-PAGE analysis of the cell lysate and soluble fraction, as well as the first IMAC step. The eluted proteins were pooled. B) SDS-PAGE analysis of the second IMAC step. After the first IMAC step, TEV protease was added and the sample was left to dialyze against ITC buffer (Table 1). SDS-PAGE analysis shows that the cleavage was complete. MBP tag and TEV were removed through another round of IMAC. C) The flow flow-through was subjected to anion exchange chromatography. Fraction 2 was collected and used for biochemical analysis. D) SDS-PAGE analysis of all GST and GST-fusion proteins used in pulldowns. GST-ATAD_SIM (36.1 kDa) was resolved on the gel close to the predicted molecular weight. ATAD_SIM (7.8 kDa), UAF1_SLD2 (13.7 kDa) and UAF1_SLD2M (13.7 kDa) were resolved at a slightly higher molecular weight than predicted.

until an appropriate NaCl concentration was reached for anion exchange chromatograph. Typically, 6 mg of protein was obtained from 0.5 L of culture. These proteins were resolved close to their predicted molecular weights during SDS-PAGE analysis and are of sufficient quality to be used in biochemical assays (Figure 16D).

GST-ATAD5_SIM was purified as per "3.1.2 Expression and Purification of GST-fusion proteins". To obtain ATAD5_SIM, GST-ATAD5_SIM was digested with His-tagged TEV at a 1:40 ratio for 2 hours at room temperature followed by 16 hours at 4 ^{o}C. The sample was then passed through pre-equilibrated cOmplete His-tag purification columns (Roche) to remove the His-tagged TEV protease and GST. ATAD5_SIM was then determined to be of sufficient quality by SDS-PAGE and stored at -80^{o}C for future use (Figure 16D).

4.2 GST pull-down assay

To determine whether or not the SIM on ATAD5 interacts to the second SLD of UAF1, a pull-down assay was performed. A positive and negative control was included. The positive control consisted of GST-p21 and PCNA, which is known to interact with each other and has been previously demonstrated (Section 3.2). The negative control consisted of GST and UAF1_SLD2, this allowed us to determine if there are any non-specific interactions between these two proteins. GST-ATAD5_SIM, GST, and GST-p21 was immobilized to the glutathione agarose resin. Excess prey proteins were then added to the immobilized bait proteins. PCNA was added to GST-p21, UAF1_SLD2 was added to GST-ATAD5_SIM and GST and UAF1_SLD2M was added to GST-ATAD5_SIM. After washing off the excess proteins, the bound proteins were eluted and analyzed by SDS-

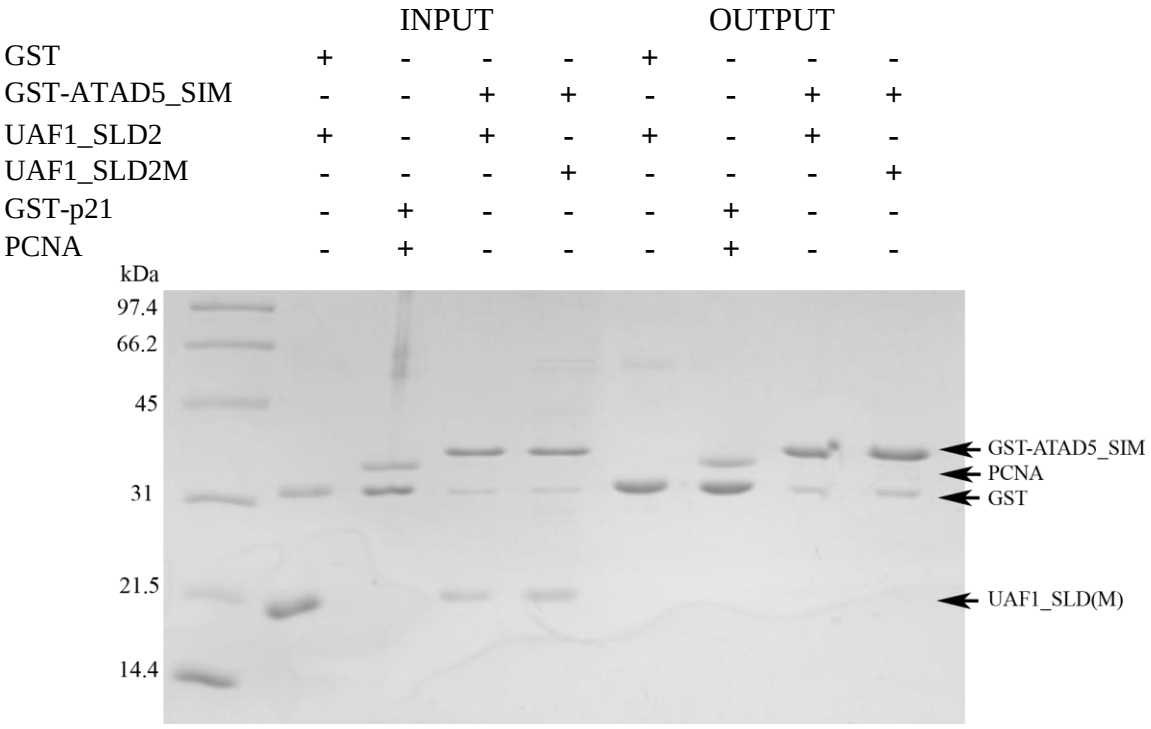

Figure 17. Interaction between ATAD5's SIM and UAF1's SLD2 cannot be detected by GST pull-down assay. Excess GST or GST-fused protein was immobilized onto 15 µL of glutathione resin. Unbound protein was then washed off and prey proteins were added in excess. After several rounds of washing, bound protein were eluted from the resin and analyzed by SDS-PAGE on a 15 % polyacrylamide gel. GST-p21 and PCNA were used as a positive control for the assay. No UAF1_SLD2 band was detected in the output.

PAGE. SDS-PAGE analysis of the elution products did not reveal any binding to occur between UAF1_SLD2 and GST-ATAD5_SIM. Neither UAF1_SLD2 or UAF1_SLD2M were present on the output lanes of the 15 % polyacrylamide gel (Figure 17). The positive and negative controls both worked however. From these results, we can speculate that the binding between these two polypeptides are too weak to be determined by this technique or that they don't interact.

4.3 Isothermal titration calorimetry

Despite not seeing an interaction between the SIM and SLD2 of ATAD5 and UAF1 respectively, ITC was used in order to confirm the interaction between these two proteins and to characterize the binding affinity. A previous study by Yang *et al.* (2011) demonstrated that UAF1 interacts with ATAD5, and loses its ability to interact upon deletion of the second SLD domain. Yang et al. (2011) detected the proteins using a co-IP assay in transfected mammalian cells, where intracellular concentrations of the proteins are relatively high (43). The pull-down assay performed may not have been able to detect the interaction due to the relatively low concentrations of proteins. Also, the pull-down assay may not be sensitive enough to detect weak protein interactions. Due to the potentially low binding affinity of the reaction, a more sensitive method is required. ITC was chosen as interactions in a wide range of binding affinities can be assessed, from milimolar to nanomolar (10^{-2} to 10^{-9} M).

ATAD5_SIM was titrated into UAF1_SLD or UAF1_SLDM in order to determine if binding between the two proteins occur and to characterize the thermodynamic parameters of the interaction. High concentrations were used since no interaction was

detected from the pull-down experiments. 1 mM of ATAD5_SIM was loaded in the syringe of the NanoITC Calorimeter (TA Instruments) and titrated into the cell containing 100 μM of UAF1_SLD or UAF1_SLDM at 25 ^{o}C. Due to the use of highly concentrated proteins, two control experiments were conducted: the first being buffer titrated into the cell containing 100 μM of UAF1_SLD and the second being 1 mM of ATAD5_SIM titrated into buffer. The titration of buffer into the cell with UAF1_SLD did not produce significant heats, however, the titration of ATAD5_SIM into buffer did (Figure 18A-B). The experimental traces were corrected by subtracting the control measurements and analyzed by NanoAnalyze (TA Instruments) using an independent binding model (Figure 18C-D). ITC measurement of the ATAD5_SIM and UAF1_SLD reaction showed a K_d of of 19.10 ± 6.48 μM, n = 0.442 ± 0.076, ΔH of -26.62 ± 7.12 kJ/mol, and a ΔS of -4.025 J/mol·K. ITC measurement of the ATAD5_SIM and UAF1_SLDM reaction showed a K_d of 77.82 ± 11.24 μM, n = 0.142 ± 0.05, ΔH of -99.95 ± 23.4 kJ/mol, and a ΔS of -256.6 J/mol·K.

From the ITC experiments, it is evident that there is an interaction between the SIM of ATAD5 and the second SLD of UAF1. Mutation of a lysine (K595E) of UAF1 in the SLD2 domain reduced the binding affinity approximately 4-fold.

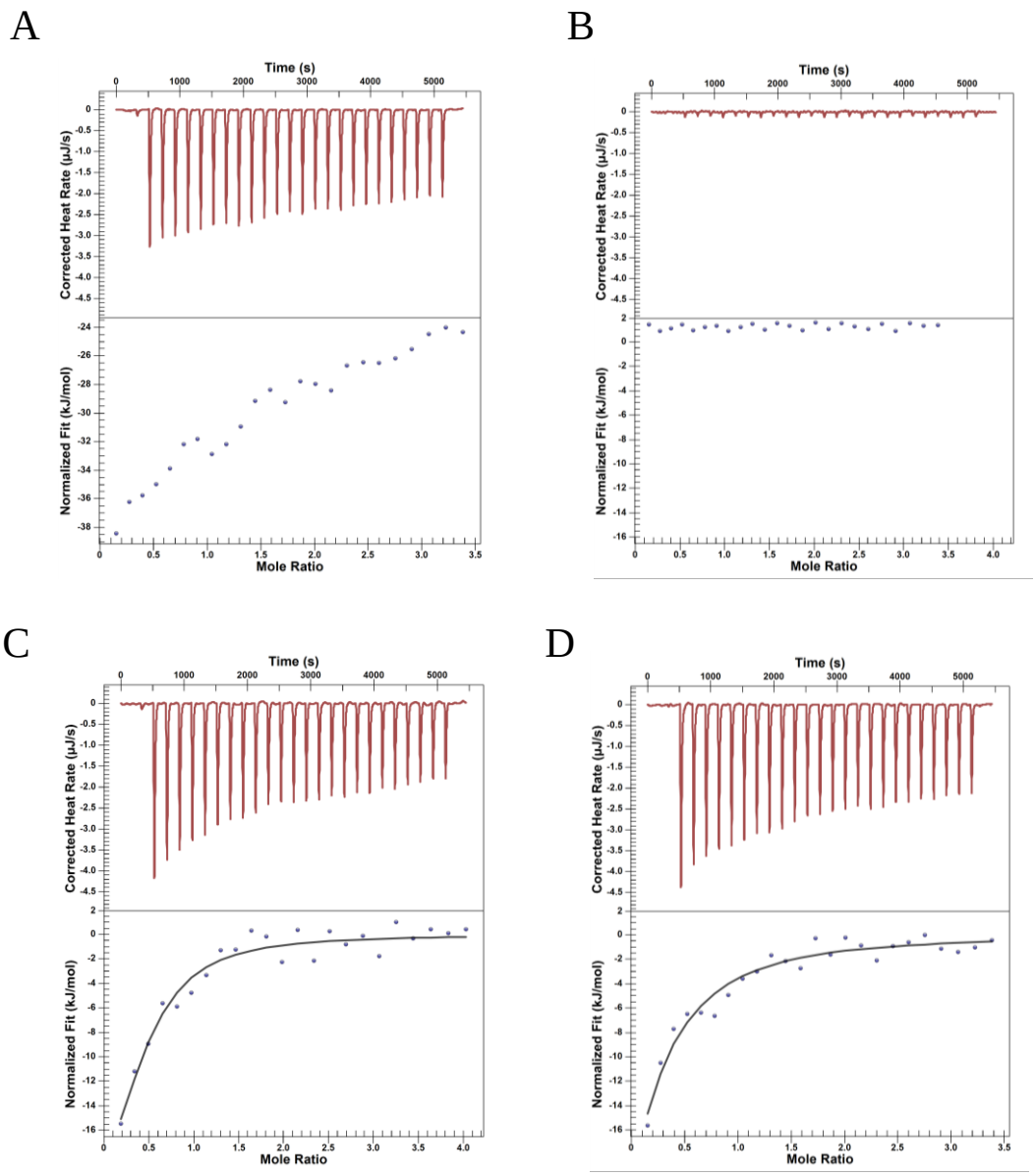

Figure 18. Determination of the thermodynamic parameters of the binding between ATAD5_SIM and UAF1_SLD2. Thermograms and experimental traces of various titrations. Buffers of proteins were exchanged by size exclusion chromatography prior to experiments. Titrations were performed stepwise in 2 µL injections followed by an initial injection of 0.48 µL at 25 ºC. A) Titration of ATAD5_SIM with buffer. B) Titration of buffer with UAF1_SLD2. C) Titration of ATAD5_SIM with UAF1_SLD2. D) Titration of ATAD5_SIM with UAF1_SLD2M.

4.2 Crystallography

Since we have established that the SIM from ATAD5 interacts with UAF1's SLD2, we wanted to characterize the structural features of the interaction, to see if it is indeed similar to the interaction between SUMO and the SUMO-interacting motif. In order to do this, crystallization trials were initiated to determine the crystallization condition for this complex. Protein from the ITC experiments were concentrated to 9 mg/mL and used in crystallization trials. The final molar ratio of ATAD5_SIM to UAF1_SLD2 was approximately 3:1. Aside from sample preparation, screening was carried out as before using a limited number of commercial crystal screen kits. A hit was observed and corresponded to the condition: 0.1 M HEPES pH 7.5, PEG 8000, 8 % ethylene glycol. One solitary hexagonal plate was observed in this condition 2 weeks after the screen was set up (Figure 19A). Longer incubation of the crystal did not encourage visible crystal growth. The crystallization of the ATAD5_SIM:UAF1_SLD2 complex in this condition could not be reproduced. Varying the concentrations of the components (precipitant, buffer pH, or protein concentration) did not produce any crystals either. IZIT dye (Hampton Research) was used in order to determine whether or not the crystal was protein, as crushing of the crystal was undesirable. The dye was able to permeate through the solvent channels of the crystal, indicating it is made of protein (Figure 19B). The crystal was mounted onto a 0.05 mm loop and streaked through the mother liquor spiked with an additional 50 % ethylene glycol and frozen in liquid nitrogen. Unfortunately, no diffraction was seen on the CMCF-081D beam line at the Canadian Light Source (figure 19D).

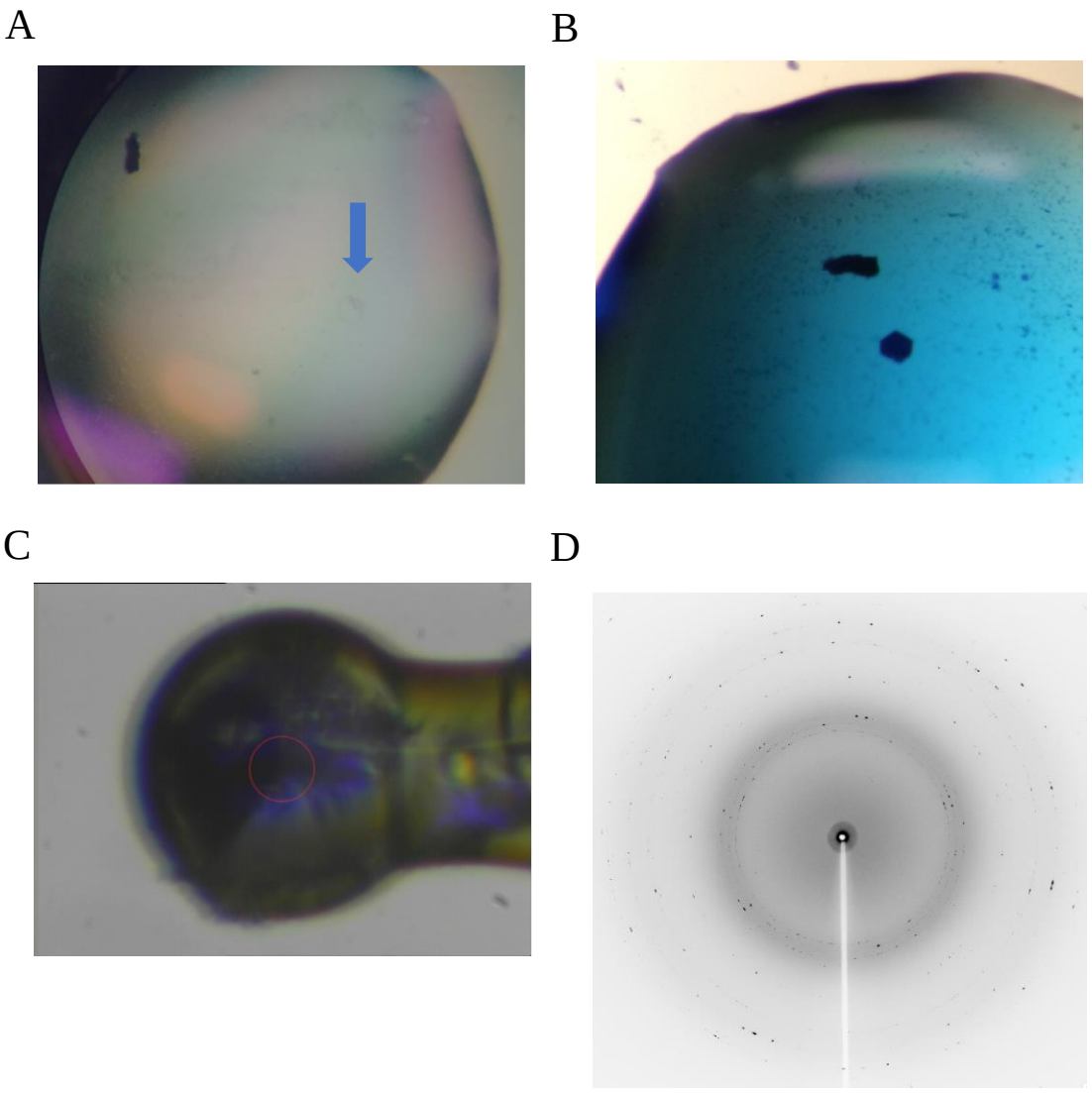

Figure 19. Crystal of the complex between ATAD5_SIM and UAF1_SLD2. A) The crystal was grown at 18 ºC from protein complex at 9 mg/mL at a ratio of 1:3 (SLD2 to SIM) in 0.1 M HEPES pH 7.5, PEG8000, 8% ethylene glycol 3 weeks after initial set up. The crystal is indicated by a blue arrow. B) Attempts to reproduce the crystal were unsuccessful so it was tested with IZIT dye. Crystal took up the dye and was stained blue. C) The crystal was mounted onto a 0.05 mm loop and treated with 30 % ethylene glycol before flash frozen in liquid nitrogen. D) Diffraction image from the crystal. No diffraction pattern was observed other than from ice.

CHAPTER 5: DISCUSSION

5.1 ATAD5 contains a PIP box motif

In this work, we have demonstrated that ATAD5 contains a PIP box motif that mediates its interaction with PCNA. Previous reports have suggested that PCNA may interact with ATAD5, however, any binding had yet to be investigated. We have identified a PIP box in the N-terminal of ATAD5 through sequence analysis that resembles that of the Y-family polymerases and rfc1 of the RFC complex. ATAD5's PIP box contains a Pro at position 1 of the consensus sequence instead of the canonical Gln and an Ile, Tyr, and Phe at positions 4, 7, and 8.

We determined that this putative PIP box motif was able to bind to PCNA using a GST pull-down assay (Section 3.2) and a yeast two-hybrid system. GST-ATAD5_PIP co-eluted with PCNA in the assay. The amount of PCNA that co-eluted with GST-APIP compared to GST-p21 was significantly lower (Figure 7). This suggests that the interaction between PCNA and the PIP box from ATAD5 is weaker than that of p21. To confirm the results of the pull-down assay, the interaction was studied in a yeast two-hybrid system. Yeast cells were transformed with plasmids expressing recombinant protein fused to either the BD or AD of the transcriptional activator protein Gal4 and spot plated to determine the phenotype of the resultant yeast. Consistent with the previous results, yeast cells co-transformed with the native N-terminal 250 amino acids of ATAD5 and PCNA showed the phenotype indicative of interaction and were able to grow on the desired selection media.

Mutation of the conserved PIP box residues (at position 4, 7, and 8) to Ala abolishes the interaction between ATAD5 and PCNA in both the GST pull-down assays, as well as the yeast two-hybrid system. The result of the experiments with the mutants agrees with

what is known about PIP box/PCNA interactions. Without the proteins that make up the "hydrophobic plug", the interactions that stabilize the PIP box in PCNA's hydrophobic pocket cannot occur.

Taken together, our results show that the putative PIP box identified interacts with PCNA, and that the conserved PIP box residues are important for interaction.

5.2 Comparing ATAD5's PIP box to other known structures

5.2.1 ATAD5 does not possess a canonical PIP box

A reason that ATAD5's PIP box was yet to be identified may be that it does not completely conform to the canonical consensus sequence (Figure 2). In the place of a Gln, there is a Pro at position 1 of the motif. There have been relatively few non-canonical PIP boxes studied where the residue at position 1 was not Gln. Many of the Y-family polymerases have non-canonical PIP Boxes and contain either a Lys (polymerase ι and polymerase κ) or a Met (polymerase η) at this position (65). The Gln from other PIP box motifs interact with the main chain carbonyl of A252 on PCNA, and a well-ordered water molecule bridges the O^{ε} of Gln and the amide-nitrogen atom of A208 at the C-terminal end of the βF_2 strand of PCNA. Kroker *et al.* (2015) identified it as the second highest contributor to p21's high binding affinity in an *in silico* alanine scanning experiment (67). In contrast, the Pro at position 1 of ATAD5's PIP box does not form any hydrogen bonds with surrounding residues or water molecules. Previous experiments where the residue at position 1 is mutated to Gln to conform to the consensus sequence, the binding affinity between the peptide and PCNA increased 4-fold (65). The presence of a Pro instead of a Gln may contribute to the lower binding affinity observed between ATAD5's PIP box and

PCNA. Proline is a proteinogenic amino acid with a secondary amine, so the α-amino group is part of the side chain. This property usually causes disruption to the secondary structure of proteins.

Interestingly, most of the polymerases that are involved in TLS do not have canonical PIP boxes and have alternative amino acids at position 1. ATAD5, which is responsible for deubiquitinating of PCNA and controlling retention of TLS polymerases on the replication fork also does not have the conserved Gln at position 1 either. There is currently no data to ascertain the significance of why these proteins involved in the DNA damage tolerance pathways contain non-canonical PIP boxes.

5.2.2 ATAD5's PIP box binds PCNA in a topologically conserved manner

The binding of ATAD5's PIP box is topologically conserved, many other crystal structures of peptides containing PIP boxes derived from other proteins in complex with PCNA show the formation of the characteristic hydrophobic plug where residues at position 4, 7, and 8 interacts with the hydrophobic pocket (47, 64, 65). Despite being predicted to be disordered, ATAD's PIP box confers a 3_{10} α-helix structure when bound to PCNA. The PIP box forms a "hydrophobic plug" that interacts with a hydrophobic pocket on PCNA (Figure 15A). Figure 20A shows a superposition of known structures of PIP box binding with PCNA. As seen in Figure 15A, hydrophobic residue I62 points towards the minor hydrophobic groove of PCNA and the two aromatic residues (Y65 and F66) point towards the major hydrophobic pocket.

The three residues at positions 4, 7, and 8 are important for the interaction with PCNA, and it has been hypothesized that the identities of these residues are responsible for

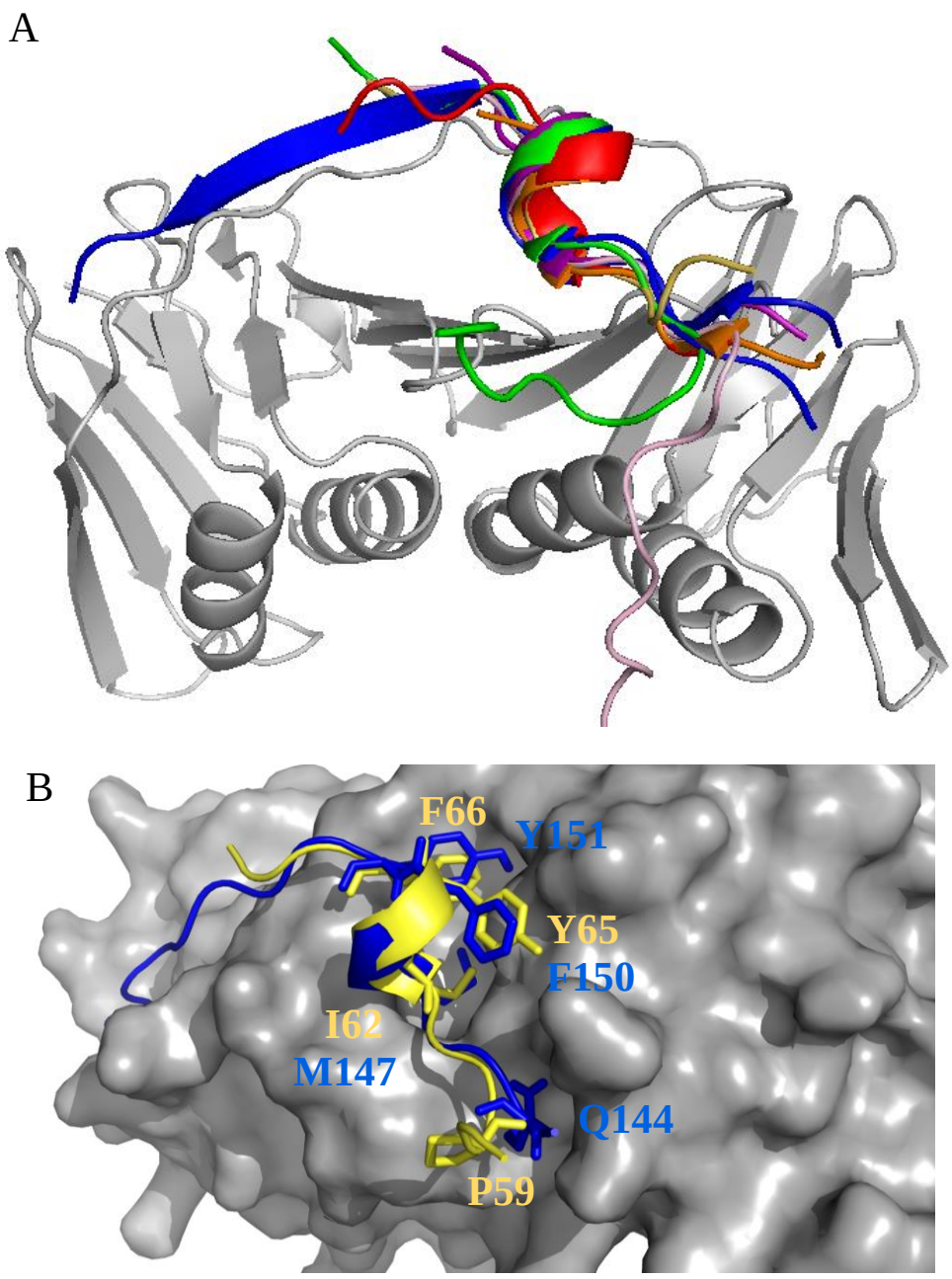

Figure 20. Comparison of human PIP box binding to PCNA. A) Cartoon representation of PCNA monomer (from this study, in gray) and the superposition of PIP boxes after structural alignment against other structures of PIP box peptides binding to PCNA. Peptide derived from ATAD5 is shown in yellow, other structures represented in this diagram are: 1U7B (red), 1U76 (orange), 2ZVK (green), 3P87 (cyan), 4RJF (blue), 4ZTD (purple) and 4D2G (pink). B) Surface representation of PCNA monomer (from this study, in gray) with cartoon representations of peptides derived from ATAD5 in yellow and p21(PDB ID: 1AXC) in blue. PIP box residues (labelled with respective colours) are represented as sticks.

tuning binding affinity (67). Comparing the binding of the hydrophobic residue from ATAD (our structure) and p21 (PDB ID: 1AXC), p21's PIP box packs tighter into the hydrophobic pocket compared to ATAD's (Figure 20B). In our structure, the nitrogen from the amine group of the Ile forms a hydrogen bond with His 44 carbonyl group's oxygen from PCNA in the two aromatic residues at position 7 and 8 forms many non-bonded contacts with many of the amino acids that make up the hydrophobic pocket of PCNA. In the p21 structure, a well-ordered water molecule helps stabilizes the interaction of the peptide with PCNA by forming many non-bonded contacts with the Tyr at position 8. Phe at this position on our structure only forms one hydrogen bond with G127 of PCNA.

The identities of the PIP box residues that form the hydrophobic plug is only one factor that affects the overall binding affinity of the PIP box peptides to PCNA. Residues can also interact with PCNA's IDCL.

5.2.3 ATAD5 peptide's interaction to the IDCL

The C-terminal of the peptide derived from ATAD5 used in our study does not have many amino acids that make contacts with the IDCL of PCNA compared to the peptide from p21. Only three residues are resolved after F66 in the C-terminal in the final structure. The remaining residues are most likely do not interact with PCNA and are hence too flexible to be seen in the structure and point toward the bulk solvent. In contrast to the p21 peptide structure, the C-terminal of the ATAD5 peptide does appear to make extensive contacts with the IDCL. In p21, the C-terminal nine amino acids form a β-strand that interacts with the IDCL. A recent article was published where *in silico* alanine scanning

identified two Arg residues four amino acid residues downstream from the last PIP box residue that contribute to p21's high binding affinity (71).

The resolved residues that follow the last PIP box residue (RKT) interact with PCNA's IDCL. Four hydrogen bonds exist here: Arg forms two hydrogen bonds with Gly 127 between an oxygen from their carboxyl and nitrogen from their amine groups. Threonine also forms two hydrogen bonds, one between its nitrogen-amine group and an oxygen from the carboxyl group of Gln 125, and the second between $O\lambda_1$ and the nitrogen amine group of Gly 127. It is interesting that the residues after position 8 form more hydrogen bonds with the IDCL of PCNA than the aromatic residues in the PIP box. Therefore, it is important to not only take into consideration the binding of the hydrophobic pocket but the IDCL as well when designing agents to inhibit PCNA binding.

5.3 UAF1 interacts with ATAD5

Prolonged replication by TLS polymerases may become a source of mutations, so regulation of their lifespan on the replication machinery is critical. Removal of ubiquitin from PCNA facilitates the switching from TLS polymerases to regular high-fidelity polymerases. ATAD5 contains a SIM in its N-terminal domain that recruits the DUB complex UAF1-USP1. We wanted to characterize this interaction to assess ATAD5's ability to act as an adapter between ubiquitinated PCNA and UAF1. ATAD5 may form a complex with UAF1 that can compete with the binding of Y-family polymerases to ubiquitinated PCNA.

5.3.1 UAF1_SLD2/ATAD5_SIM interaction was not detectable in affinity pull-down assay

The interaction between ATAD5's SIM and UAF1's second SLD could not be detected in our affinity pull-down assays. No interaction was detected as UAF1's SLD2 did not co-eluted with GST fused to ATAD5's SIM. There are several reasons for this occurrence. Firstly, the GST-affinity pull-down technique is more suited for stronger interactions, weak or transient interactions may not be detected by this method. Secondly, the cloned portion of the SIM is not sufficient to facilitate interaction, only 39 amino acids (the SIM was flanked by ten amino acids) were amplified out of ATAD5; this may not be enough for it to fold correctly. Lastly, Yang *et al.* (2011) studied this interaction using co-IP experiments using extracts from cells transfected with the proteins of interest (where intercellular concentrations were high) (43). Additional cofactors may be present in the cell extract that facilitates the binding.

5.3.2 ITC reveals µM binding between UAF1_SLD2 and ATAD5_SIM

Despite not seeing a positive result from the pull-down assays, the interaction between ATAD5_SIM and UAF1_SLD2 was determined to have a K_d of 19.1 ± 6.48 µM. ITC experiments can detect a wide range of binding affinities (from nM to mM). With the assumption that the protein is weak (from the GST pull-down experiments), we used high concentrations of proteins. ATAD5_SIM was loaded into the syringe and titrated into a cell containing UAF1_SLD2. The K_d of this reaction was approximately 3-4 fold lower than the ATAD5 PIP box/PCNA interaction. The binding affinity seen in the ITC experiments were not completely unexpected. Lee *et al.* (2010) found that the chromatin-

bound USP1 level was not changed after *ELG1* knockdown and USP1 or UAF1 foci was not formed in response to DNA damage (72). Mutation of a lysine important for the interaction between ATAD5 and UAF1 resulted in a 4-fold reduction in binding affinity, the dissociation constant of this reaction was found to be 77.82 ± 11.24 μM. This result agrees with the observations made by Yang et al. (2011) where they observed a reduction in ATAD5 binding to UAF1 bearing the same mutation (43).

We were able to determine that UAF1 binds to ATAD5's SIM in the low μM range. The binding affinity between these proteins is reduced upon mutation of a lysine on UAF1. Our experiments contribute to the confirmation that the binding between the SLD2 sequence of UAF1 with ATAD5's SIM has conserved binding characteristics to known SUMO/SIM interactions previously described in the literature (73).

5.4 Functional implications

Many proteins interact with PCNA by the way of the PIP box motif. Almost 200 different biological PIP boxes have been proposed from a bioinformatics analysis. From the data available, not all PIP boxes interact with the same affinity (Table 5). The variations of the amino acid at each position allows for the "tuning" of the binding affinities, possibly linking it to the protein's function (67). What guides the binding of various proteins to PCNA during different pathways is unclear, as PIP boxes binding to PCNA's hydrophobic pocket with low affinity can be displaced those of higher affinity, such as p21's PIP box (47).

PCNA-PIP box interactions may not have been optimized for high affinity during evolution. PCNA is thought to be a "toolbelt" for replication machinery, allowing multiple

Table 5. Summary of PIP box-containing peptides from crystal structures available from the Protein Data Bank (www.pdb.org). Positions 1, 4, 7 and 8 of the PIP box consensus sequence are bolded.

PDB ID	Author	Peptide Sequence	K_d	Ligand	Notes
4ZTD	S. Hoffmann(69)	KQRVRVKTVPSLF**Q**AK**L**DT**FL**WS	30.7 µM	TRAIP	
4RJF	A. Kroker(67)	GRKRR**Q**TS**M**TD**FY**HSKRRLIFS	82.6 nM	CDK1	
4D2G	A. De Biasio(68)	GNPVCVRPTPKW**Q**KG**I**GE**FF**RLS PKDSE	5.56 µM	P15	
3P87	D. Bubeck(66)	DKSG**M**KS**I**DT**FF**GVKNKKKIGKV	N/A	RNASEH2B	
2ZVL	A. Hishiki(65)	CIKPNNP**K**HT**L**DI**FF**KPLTH	4.9µM	Polκ	
2ZVM	A. Hishiki(65)	CAK**K**GL**I**DY**YL**MPSLST	0.29 µM	Polι	
2ZVK	A. Hishiki(65)	CKRPRPEG**M**QT**L**ES**FF**KPLTH	0.4 µM	Polη	
1U76	J. Bruning(64)	KANR**Q**VS**I**TG**FF**QRK	15.6 µM	P66	1.53 µM with QRKRRLIFS added to C terminal
1U7B	J. Bruning(64)	SRQGST**Q**GR**L**DD**FF**KVTGSL	60.0 µM	FEN1	
1AXC	J. Gulbis(47)	GRKRR**Q**TS**M**TD**FY**HSKRRLIFS	82.6 nM	P21	
1VYJ	G. Kontopidis(70)	SAVL**Q**KK**I**TD**YF**HPKK	100 nM	PL	
	T. Bui	APPL**P**SN**I**LD**YF**RKTSPT	6.17 µM	ATAD5	From this study.

different proteins of the same pathway to bind. The low binding affinities afford the components (or tools) to be changed on the PCNA (toolbelt) scaffold, allowing it to facilitate a wide variety of functions while maintaining the hierarchy of binding.

Bruning et al. (2004) reported that the PIP box from p66, a subunit of polδ, binds to PCNA with an affinity of 15.6 μM (64). Additional contacts outside of the PIP boxes exists. In vitro studies have shown that most replicative DNA polymerases have nanomolar affinity for the primer-template junction of DNA, but significantly less affinity for duplex. Polδ has significantly higher affinity for PCNA when it is loaded onto DNA due to the additive effects of the PIP box interaction. Reaching a lesion on DNA and stalling of the replication fork may disrupt its interaction with DNA, allowing other "tools" to replace polδ to make repairs.

Some proteins have other domains that interact with PCNA when it is modified. For example, many of the Y-family polymerases contain additional ubiquitin-binding motifs (UBMs) in the form of ubiquitin binding zinc fingers (UBZs). These UBMs may allow the Y-family polymerases to bind to PCNA in place of existing proteins at stalled replication forks (where PCNA is monoubiquitinated). Even without the aid of the UBZ motif, the PIP-Boxes from Y-family polymerases have been reported to bind from 4.9 μM up to 290 nM (Table 5). The additional binding between the UBMs and ubiquitin may facilitate the exchange of polymerases with the normal high-fidelity ones.

We have determined that ATAD5's PIP box binds to PCNA with low μM affinity (6.17 ± 0.78 μM). Since ATAD5 is also known to recruit the UAF1-USP1 DUB complex and knockdown of ATAD5 causes an accumulation of ubiquitinated PCNA on chromatin, we wanted to determine if it directly interacts with ubiquitin. We tested whether or not

ATAD5 contains a ubiquitin-binding domain using a yeast two-hybrid system and *in silico* sequence analysis. There did not appear to be any interaction between ATAD5 and ubiquitin (data not shown). As an adapter, the combination of ATAD5's PIP box/PCNA and SIM/UAF1 interactions may be strong enough to displace the TLS polymerase from the replication fork after TLS, allowing the ubiquitin to be removed and normal high-fidelity polymerases to continue replication.

5.5 Conclusion and future directions

We hypothesized that ATAD5 acts an adaptor that interacts with PCNA and UAF1. Although we did not assess whether or not ATAD5 was able to interact with these two proteins at the same time, we were able to characterize the interaction between its PIP box and SIM with PCNA and UAF1's SLD2. In our study, we have demonstrated that ATAD5 contains a PIP box and that it interacts with PCNA in the low micromolar range. Based on the comparison of PIP boxes from other human proteins, we can see that the residues that make up the hydrophobic plug are important for tuning the affinity of the peptide towards PCNA. Interactions with the IDCL are also important for binding affinity. Furthermore, we were able to characterize an interaction between ATAD5 and UAF1.

A SIM on the N-terminal of ATAD5 interacts with the second SLD from UAF1. We have determined that the interaction between these two polypeptides have a binding affinity of 20 μM. A mutation on a lysine (K595) to Glu in the second SLD of UAF1 reduced its binding affinity to PCNA 3-fold. Yang *et al.* (2011) initially made this mutation based off of a model of the SLD2 domain with SUMO-2, as the corresponding lysine is critical in SUMO/SIM interactions. The SUMO moiety of sumoylated proteins is able to

mediate enzyme-substrate interactions and is found in many protein pathways (73). ATAD5's SIM may also interact with other sumo-modified proteins. It would be interesting to assess whether or not ATAD5's SIM is able to interact with SUMO1-4 or if it is similar to FANCDI's (another substrate of the UAF1-USP1 DUB) SIM, which exclusively interacts with SLDs. Finally, a crystal structure of the complex formed between the SIM of ATAD5 and SLD2 of UAF1 could provide mechanistic insight on how similar (if at all) it is to SIM-SUMO interactions.

ATAD5 functions to recruit the UAF1-USP1 DUB complex to monoubiquitinated PCNA, however, it also functions to unload PCNA during DNA replication. These two functions are probably separate as previous studies have demonstrated that formation of the RFC-like complex containing ATAD5 is not required to control levels of PCNA ubiquitination. The C-terminal is responsible for ATAD5's association with RFC subunits, however, the N-terminal 500 amino acids of ATAD5 alone, is sufficient to reduce levels of monoubiquitinated PCNA. It is unlikely that the PCNA unloading by the RFC-like complex containing ATAD5 is required in order to deubiquitinate PCNA (72). Previous reports have knocked down ATAD5 or used partial ATAD5 fragments in their studies (32, 41). With the knowledge of the residues responsible for the interaction between ATAD5 and PCNA, mutations can be made to the full-length protein and studied. Similar phenotypes to ATAD5 knockdown cells are expected upon DNA damage by DNA alkylating agents or ionizing radiation. Cells expressing mutant ATAD5 will have an impaired DNA damage response, leading to increased cell death. More specifically, monoubiquitinated PCNA will accumulate on chromatin, leading to increased mutation rates due to prolonged replication by Y-family polymerases and gross genomic instability.

Furthermore, inactive replication factories will begin to accumulate on DNA and prevent cell replication and eventually lead to cell death.

Knowledge of how each residue of the PIP box, as well as the flanking residues, interact with PCNA will allow us to develop more effective drugs to combat cancer. Inhibition of PCNA at the mRNA and protein level has been shown to inhibit proliferation and cell growth, sensitizing cancer cells to chemotherapeutic agents. However, no clinical trials are being conducted on inhibitors of PCNA. Current inhibitors often have low potency, cell permeability, bioavailability, and undesirable off-target effects (67). A more thorough understanding of the binding between PCNA and its many binding partners will allow for effective inhibitors to be developed.

REFERENCES

1. McCulloch, S. D., and Kunkel, T. A. (2008) The fidelity of DNA synthesis by eukaryotic replicative and translesion synthesis polymerases. *Cell Res.* **18**, 148–161
2. Fuchs, R. P., and Pagès, V. (2003) Uncoupling of Leading- and Lagging-Strand DNA Replication During Lesion Bypass in Vivo. *Science*. **300**, 1300–1303
3. Cox, M. M., Goodman, M. F., Kreuzer, K. N., Sherratt, D. J., Sandler, S. J., and Marians, K. J. (2000) The importance of repairing stalled replication forks. *Nature*. **404**, 37–41
4. Friedberg, E. C. (2005) Suffering in silence: the tolerance of DNA damage. *Nat. Rev. Mol. Cell Biol.* **6**, 943–953
5. Ohmori, H., Friedberg, E. C., Fuchs, R. P. P., Goodman, M. F., Hanaoka, F., Hinkle, D., Kunkel, T. A., Lawrence, C. W., Livneh, Z., Nohmi, T., Prakash, L., Prakash, S., Todo, T., Walker, G. C., Wang, Z., and Woodgate, R. (2001) The Y-Family of DNA Polymerases. *Mol. Cell*. **8**, 7–8
6. Sale, J. E., Lehmann, A. R., and Woodgate, R. (2012) Y-family DNA polymerases and their role in tolerance of cellular DNA damage. *Nat. Rev. Mol. Cell Biol.* **13**, 141–152
7. Lehmann, A. R., Niimi, A., Ogi, T., Brown, S., Sabbioneda, S., Wing, J. F., Kannouche, P. L., and Green, C. M. (2007) Translesion synthesis: Y-family polymerases and the polymerase switch. *DNA Repair*. **6**, 891–899
8. Miyachi, K., Fritzler, M. J., and Tan, E. M. (1978) Autoantibody to a Nuclear Antigen in Proliferating Cells. *J. Immunol.* **121**, 2228–2234
9. Bravo, R., and Celis, J. E. (1980) A search for differential polypeptide synthesis throughout the cell cycle of HeLa cells. *J. Cell Biol.* **84**, 795–802
10. Mathews, M. B., Bernstein, R. M., Franza, B. R., and Garrels, J. I. (1984) Identity of the proliferating cell nuclear antigen and cyclin. *Nature*. **309**, 374–376
11. Kelman, Z. (1997) PCNA: structure, functions and interactions. *Publ. Online 07 Febr. 1997 Doi101038sjonc1200886*. 10.1038/sj.onc.1200886

12. Majka, J., and Burgers, P. M. . (2004) The PCNA–RFC Families of DNA Clamps and Clamp Loaders. in *Progress in Nucleic Acid Research and Molecular Biology*, pp. 227–260, Academic Press, **Volume 78**, 227–260
13. Stukenberg, P. T., Studwell-Vaughan, P. S., and O'Donnell, M. (1991) Mechanism of the sliding beta-clamp of DNA polymerase III holoenzyme. *J. Biol. Chem.* **266**, 11328–11334
14. Kong, X.-P., Onrust, R., O'Donnell, M., and Kuriyan, J. (1992) Three-dimensional structure of the β subunit of E. coli DNA polymerase III holoenzyme: A sliding DNA clamp. *Cell*. **69**, 425–437
15. Gulbis, J. M., Kelman, Z., Hurwitz, J., O'Donnell, M., and Kuriyan, J. (1996) Structure of the C-Terminal Region of p21WAF1/CIP1 Complexed with Human PCNA. *Cell*. **87**, 297–306
16. Jonsson, Z. O. (1998) Regulation of DNA replication and repair proteins through interaction with the front side of proliferating cell nuclear antigen. *EMBO J.* **17**, 2412–2425
17. Warbrick, E. (1998) PCNA BINDING THROUGH A CONSERVED MOTIF. *BioEssays*. **20**, 195–199
18. Xu, H., Zhang, P., Liu, L., and Lee, M. Y. W. T. (2001) A Novel PCNA-Binding Motif Identified by the Panning of a Random Peptide Display Library. *Biochemistry (Mosc.)*. **40**, 4512–4520
19. Wade Harper, J., Adami, G. R., Wei, N., Keyomarsi, K., and Elledge, S. J. (1993) The p21 Cdk-interacting protein Cip1 is a potent inhibitor of G1 cyclin-dependent kinases. *Cell*. **75**, 805–816
20. Bruning, J. B., and Shamoo, Y. (2004) Structural and Thermodynamic Analysis of Human PCNA with Peptides Derived from DNA Polymerase-δ p66 Subunit and Flap Endonuclease-1. *Structure*. **12**, 2209–2219
21. Moldovan, G.-L., Pfander, B., and Jentsch, S. (2007) PCNA, the Maestro of the Replication Fork. *Cell*. **129**, 665–679
22. Dieckman, L. M., Freudenthal, B. D., and Washington, M. T. (2012) PCNA Structure and Function: Insights from Structures of PCNA Complexes and Post-translationally Modified PCNA. in *The Eukaryotic Replisome: a Guide to Protein Structure and*

Function (MacNeill, S. ed), pp. 281–299, Subcellular Biochemistry, Springer Netherlands, [online] http://link.springer.com/chapter/10.1007/978-94-007-4572-8_15 (Accessed March 24, 2016)

23. Dionne, I., Robinson, N. P., McGeoch, A. T., Marsh, V. L., Reddish, A., and Bell, S. D. (2003) DNA replication in the hyperthermophilic archaeon Sulfolobus solfataricus. *Biochem. Soc. Trans.* **31**, 674–676
24. Lee, K., and Myung, K. (2008) PCNA Modifications for Regulation of Post-Replication Repair Pathways. *Mol. Cells*. **26**, 5–11
25. Hoege, C., Pfander, B., Moldovan, G.-L., Pyrowolakis, G., and Jentsch, S. (2002) RAD6-dependent DNA repair is linked to modification of PCNA by ubiquitin and SUMO. *Nature*. **419**, 135–141
26. Pfander, B., Moldovan, G.-L., Sacher, M., Hoege, C., and Jentsch, S. (2005) SUMO-modified PCNA recruits Srs2 to prevent recombination during S phase. *Nature*. **436**, 428–433
27. Parie Garg, P. M. B. (2006) Garg, P. & Burgers, P. M. Ubiquitinated proliferating cell nuclear antigen activates translesion DNA polymerases and REV1. Proc. Natl Acad. Sci. USA 102, 18361-18366. *Proc. Natl. Acad. Sci. U. S. A.* **102**, 18361–6
28. Zhuang, Z., Johnson, R. E., Haracska, L., Prakash, L., Prakash, S., and Benkovic, S. J. (2008) Regulation of polymerase exchange between Polη and Polδ by monoubiquitination of PCNA and the movement of DNA polymerase holoenzyme. *Proc. Natl. Acad. Sci. U. S. A.* **105**, 5361–5366
29. Huang, T. T., Nijman, S. M. B., Mirchandani, K. D., Galardy, P. J., Cohn, M. A., Haas, W., Gygi, S. P., Ploegh, H. L., Bernards, R., and D'Andrea, A. D. (2006) Regulation of monoubiquitinated PCNA by DUB autocleavage. *Nat. Cell Biol.* **8**, 341–347
30. Nijman, S. M. B., Luna-Vargas, M. P. A., Velds, A., Brummelkamp, T. R., Dirac, A. M. G., Sixma, T. K., and Bernards, R. (2005) A Genomic and Functional Inventory of Deubiquitinating Enzymes. *Cell*. **123**, 773–786

31. Cohn, M. A., Kowal, P., Yang, K., Haas, W., Huang, T. T., Gygi, S. P., and D'Andrea, A. D. (2007) A UAF1-Containing Multisubunit Protein Complex Regulates the Fanconi Anemia Pathway. *Mol. Cell*. **28**, 786–797
32. Lee, K., Yang, K., Cohn, M. A., Sikdar, N., D'Andrea, A. D., and Myung, K. (2010) Human ELG1 Regulates the Level of Ubiquitinated Proliferating Cell Nuclear Antigen (PCNA) through Its Interactions with PCNA and USP1. *J. Biol. Chem.* **285**, 10362–10369
33. Cohn, M. A., Kee, Y., Haas, W., Gygi, S. P., and D'Andrea, A. D. (2009) UAF1 Is a Subunit of Multiple Deubiquitinating Enzyme Complexes. *J. Biol. Chem.* **284**, 5343–5351
34. Kubota, T., Myung, K., and Donaldson, A. D. (2013) Is PCNA unloading the central function of the Elg1/ATAD5 replication factor C-like complex? *Cell Cycle*. **12**, 2570–2579
35. Scholes, D. T., Banerjee, M., Bowen, B., and Curcio, M. J. (2001) Multiple Regulators of Ty1 Transposition in Saccharomyces cerevisiae Have Conserved Roles in Genome Maintenance. *Genetics*. **159**, 1449–1465
36. Smith, S., Hwang, J.-Y., Banerjee, S., Majeed, A., Gupta, A., and Myung, K. (2004) Mutator genes for suppression of gross chromosomal rearrangements identified by a genome-wide screening in Saccharomyces cerevisiae. *Proc. Natl. Acad. Sci. U. S. A.* **101**, 9039–9044
37. Banerjee, S., Sikdar, N., and Myung, K. (2007) Suppression of gross chromosomal rearrangements by a new alternative replication factor C complex. *Biochem. Biophys. Res. Commun.* **362**, 546–549
38. Kubota, T., Katou, Y., Nakato, R., Shirahige, K., and Donaldson, A. D. (2015) Replication-Coupled PCNA Unloading by the Elg1 Complex Occurs Genome-wide and Requires Okazaki Fragment Ligation. *Cell Rep.* **12**, 774–787
39. Sikdar, N., Banerjee, S., Lee, K., Wincovitch, S., Pak, E., Nakanishi, K., Jasin, M., Dutra, A., and Myung, K. (2009) DNA damage responses by human ELG1 in S phase are important to maintain genomic integrity. *Cell Cycle Georget. Tex*. **8**, 3199–3207
40. Bell, D. W., Sikdar, N., Lee, K., Price, J. C., Chatterjee, R., Park, H.-D., Fox, J., Ishiai, M., Rudd, M. L., Pollock, L. M., Fogoros, S. K., Mohamed, H., Hanigan, C. L.,

Program, N. C. S., Zhang, S., Cruz, P., Renaud, G., Hansen, N. F., Cherukuri, P. F., Borate, B., McManus, K. J., Stoepel, J., Sipahimalani, P., Godwin, A. K., Sgroi, D. C., Merino, M. J., Elliot, G., Elkahloun, A., Vinson, C., Takata, M., Mullikin, J. C., Wolfsberg, T. G., Hieter, P., Lim, D.-S., and Myung, K. (2011) Predisposition to Cancer Caused by Genetic and Functional Defects of Mammalian Atad5. *PLOS Genet*. **7**, e1002245

41. Lee, K., Fu, H., Aladjem, M. I., and Myung, K. (2013) ATAD5 regulates the lifespan of DNA replication factories by modulating PCNA level on the chromatin. *J. Cell Biol.* **200**, 31–44
42. Kerscher, O. (2007) SUMO junction—what's your function? *EMBO Rep.* **8**, 550–555
43. Yang, K., Moldovan, G.-L., Vinciguerra, P., Murai, J., Takeda, S., and D'Andrea, A. D. (2011) Regulation of the Fanconi anemia pathway by a SUMO-like delivery network. *Genes Dev.* **25**, 1847–1858
44. Sambrook, J., and Russell, D. W. (2001) *Molecular Cloning: a laboratory manual*, 3rd Ed., Cold Spring Harbor Laboratory Press, Cold Sping Harbor, New York
45. Aiyar, A., Xiang, Y., and Leis, J. (1996) Site-Directed Mutagenesis Using Overlap Extension PCR. in *In Vitro Mutagenesis Protocols* (Trower, M. ed), pp. 177–191, Methods In Molecular Medicine™, Humana Press, [online] http://dx.doi.org/10.1385/0-89603-332-5%3A177 (Accessed May 3, 2016)
46. Klock, H., and Lesley, S. (2009) The Polymerase Incomplete Primer Extension (PIPE) Method Applied to High-Throughput Cloning and Site-Directed Mutagenesis. in *High Throughput Protein Expression and Purification* (Doyle, S. ed), pp. 91–103, Methods in Molecular Biology, Humana Press, [online] http://dx.doi.org/10.1007/978-1-59745-196-3_6 (Accessed May 3, 2016)
47. Gulbis, J. M., Kelman, Z., Hurwitz, J., O'Donnell, M., and Kuriyan, J. (1996) Structure of the C-Terminal Region of p21WAF1/CIP1 Complexed with Human PCNA. *Cell*. **87**, 297–306
48. Inoue, H., Nojima, H., and Okayama, H. (1990) High efficiency transformation of Escherichia coli with plasmids. *Gene*. **96**, 23–28

49. James, P., Halladay, J., and Craig, E. A. (1996) Genomic Libraries and a Host Strain Designed for Highly Efficient Two-Hybrid Selection in Yeast. *Genetics*. **144**, 1425–1436
50. Daniel Gietz, R., and Woods, R. A. (2002) Transformation of yeast by lithium acetate/single-stranded carrier DNA/polyethylene glycol method. in *Methods in Enzymology* (Fink, C. G. and G. R. ed), pp. 87–96, Guide to Yeast Genetics and Molecular and Cell Biology - Part B, Academic Press, **350**, 87–96
51. Battye, T. G. G., Kontogiannis, L., Johnson, O., Powell, H. R., and Leslie, A. G. (2011) iMOSFLM: a new graphical interface for diffraction-image processing with MOSFLM. *Acta Crystallogr. D Biol. Crystallogr.* **67**, 271–281
52. Winn, M. D., Ballard, C. C., Cowtan, K. D., Dodson, E. J., Emsley, P., Evans, P. R., Keegan, R. M., Krissinel, E. B., Leslie, A. G. W., McCoy, A., McNicholas, S. J., Murshudov, G. N., Pannu, N. S., Potterton, E. A., Powell, H. R., Read, R. J., Vagin, A., and Wilson, K. S. (2011) Overview of the CCP4 suite and current developments. *Acta Crystallogr. D Biol. Crystallogr.* **67**, 235–242
53. EVANS, P. (1997) Scala. *Med. Res. Counc. CCP 4 Newsl. Protein Crystallogr.*
54. Padilla, J. E., and Yeates, T. O. (2003) A statistic for local intensity differences: robustness to anisotropy and pseudo-centering and utility for detecting twinning. *Acta Crystallogr. D Biol. Crystallogr.* **59**, 1124–1130
55. McCoy, A. J., Grosse-Kunstleve, R. W., Adams, P. D., Winn, M. D., Storoni, L. C., and Read, R. J. (2007) Phaser crystallographic software. *J. Appl. Crystallogr.* **40**, 658–674
56. Winn, M. D., Isupov, M. N., and Murshudov, G. N. (2001) Use of TLS parameters to model anisotropic displacements in macromolecular refinement. *Acta Crystallogr. D Biol. Crystallogr.* **57**, 122–133
57. Emsley, P., and Cowtan, K. (2004) *Coot* : model-building tools for molecular graphics. *Acta Crystallogr. D Biol. Crystallogr.* **60**, 2126–2132
58. Kawasaki, T. (1991) Hydroxyapatite as a liquid chromatographic packing. *J. Chromatogr. A.* **544**, 147–184

59. Castillo, A. G., Collinet, D., Deret, S., Kashoggi, A., and Bejarano, E. R. (2003) Dual interaction of plant PCNA with geminivirus replication accessory protein (Ren) and viral replication protein (Rep). *Virology*. **312**, 381–394
60. Frampton, J., Irmisch, A., Green, C. M., Neiss, A., Trickey, M., Ulrich, H. D., Furuya, K., Watts, F. Z., Carr, A. M., and Lehmann, A. R. (2006) Postreplication Repair and PCNA Modification in Schizosaccharomyces pombe. *Mol. Biol. Cell*. **17**, 2976–2985
61. Luban, J., and Goff, S. P. (1995) The yeast two-hybrid system for studying protein—protein interactions. *Curr. Opin. Biotechnol.* **6**, 59–64
62. Fields, S., and Song, O. (1989) A novel genetic system to detect protein–protein interactions. *Nature*. **340**, 245–246
63. Leavitt, S., and Freire, E. (2001) Direct measurement of protein binding energetics by isothermal titration calorimetry. *Curr. Opin. Struct. Biol.* **11**, 560–566
64. Bruning, J. B., and Shamoo, Y. (2004) Structural and Thermodynamic Analysis of Human PCNA with Peptides Derived from DNA Polymerase-δ p66 Subunit and Flap Endonuclease-1. *Structure*. **12**, 2209–2219
65. Hishiki, A., Hashimoto, H., Hanafusa, T., Kamei, K., Ohashi, E., Shimizu, T., Ohmori, H., and Sato, M. (2009) Structural Basis for Novel Interactions between Human Translesion Synthesis Polymerases and Proliferating Cell Nuclear Antigen. *J. Biol. Chem.* **284**, 10552–10560
66. Bubeck, D., Reijns, M. A. M., Graham, S. C., Astell, K. R., Jones, E. Y., and Jackson, A. P. (2011) PCNA directs type 2 RNase H activity on DNA replication and repair substrates. *Nucleic Acids Res.* 10.1093/nar/gkq980
67. Kroker, A. J., and Bruning, J. B. (2015) p21 Exploits Residue Tyr151 as a Tether for High-Affinity PCNA Binding. *Biochemistry (Mosc.)*. **54**, 3483–3493
68. De Biasio, A., de Opakua, A. I., Mortuza, G. B., Molina, R., Cordeiro, T. N., Castillo, F., Villate, M., Merino, N., Delgado, S., Gil-Cartón, D., Luque, I., Diercks, T., Bernadó, P., Montoya, G., and Blanco, F. J. (2015) Structure of p15PAF–PCNA complex and implications for clamp sliding during DNA replication and repair. *Nat. Commun.* **6**, 6439
69. Hoffmann, S., Smedegaard, S., Nakamura, K., Mortuza, G. B., Räschle, M., Opakua, A. I. de, Oka, Y., Feng, Y., Blanco, F. J., Mann, M., Montoya, G., Groth, A., Bekker-

Jensen, S., and Mailand, N. (2016) TRAIP is a PCNA-binding ubiquitin ligase that protects genome stability after replication stress. *J. Cell Biol.* **212**, 63–75

70. Kontopidis, G., Wu, S.-Y., Zheleva, D. I., Taylor, P., McInnes, C., Lane, D. P., Fischer, P. M., and Walkinshaw, M. D. (2005) Structural and biochemical studies of human proliferating cell nuclear antigen complexes provide a rationale for cyclin association and inhibitor design. *Proc. Natl. Acad. Sci. U. S. A.* **102**, 1871–1876
71. Kroker, A. J., and Bruning, J. B. (2015) p21 Exploits Residue Tyr151 as a Tether for High-Affinity PCNA Binding. *Biochemistry (Mosc.)*. **54**, 3483–3493
72. Lee, K., Yang, K., Cohn, M. A., Sikdar, N., D'Andrea, A. D., and Myung, K. (2010) Human ELG1 Regulates the Level of Ubiquitinated Proliferating Cell Nuclear Antigen (PCNA) through Its Interactions with PCNA and USP1. *J. Biol. Chem.* **285**, 10362–10369
73. Hecker, C.-M., Rabiller, M., Haglund, K., Bayer, P., and Dikic, I. (2006) Specification of SUMO1- and SUMO2-interacting Motifs. *J. Biol. Chem.* **281**, 16117–16127

APPENDIX

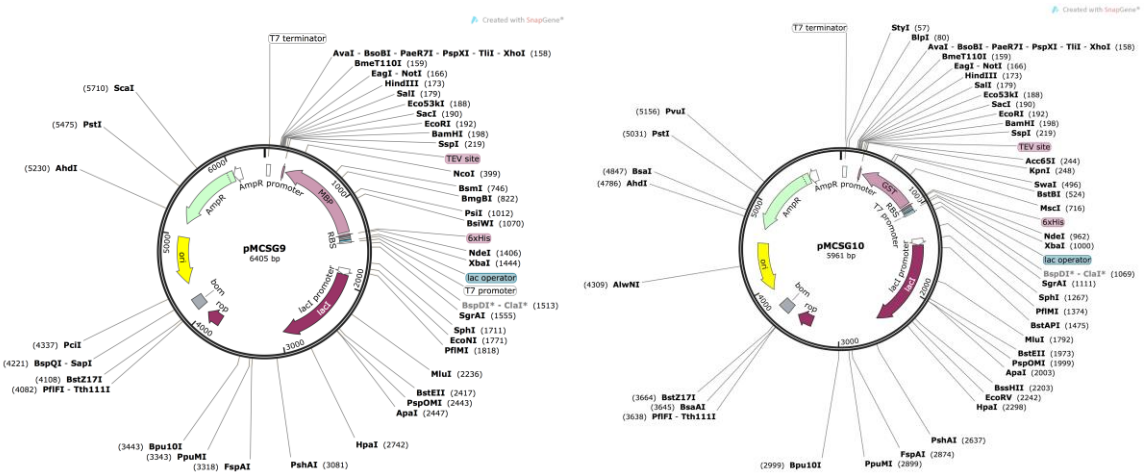

Figure I. Vector map of pMCSG9 (left) and pMCSG10 (right). Unique restriction enzyme cutting sites are indicated along with notable features of the plasmid. Maps were created with SnapGene Viewer.

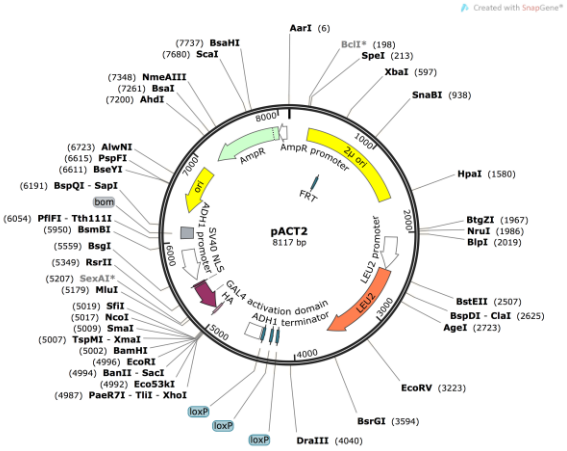

Figure II. Vector map of pACT2. Unique restriction enzyme cutting sites are indicated along with notable features of the plasmid. Maps were created with SnapGene Viewer.

VITA

Name:	Tam T. Bui
Post-Secondary Education and Degrees	The University of Western Ontario London, Ontario, Canada 2013-2016 The University of Guelph Guelph, Ontario, Canada 2008-2013
Conferences and External Courses	Poster Presenter IUCR 23rd Congress Montreal, Ontario, Canada 2014 Student EMBO High Throughput Protein Crystallization Marseille, France 2015 Poster Presenter London Health Research Day London, Ontario, Canada 2016
Honours and Awards	Western Graduate Research Scholarship (2013-2015) Larry Calvert CNC/IUCr Trust Fund Award (2014)
Related Work Experience	Research Technician Dr. Rod Merrill The University of Guelph Guelph, Ontario, Canada 2012-2013 R&D Research Assistant McNeil Consumer Healthcare Guelph, Ontario, Canada 2011